Correction date: 20.10.2022.

Slyudyankaite, $Na_{28}Ca_4(Si_{24}Al_{24}O_{96})(SO_4)_6(S_6)_{1/3}(CO_2)\cdot 2H_2O$, a new sodalite-group mineral from the Malo-Bystrinskoe lazurite deposit, Baikal Lake area, Russia

ANATOLY N. SAPOZHNIKOV[1], NADEZHDA B. BOLOTINA[2], NIKITA V. CHUKANOV[3,4], ROMAN YU. SHENDRIK[1], EKATERINA V. KANEVA[1], MARINA F. VIGASINA[4], LARISA A. IVANOVA[5], VLADIMIR L. TAUSON[1], AND SERGEY V. LIPKO[1]

[1]Vinogradov Institute of Geochemistry, Siberian Branch of Russian Academy of Sciences, Favorskii Street 1a, Irkutsk, 664033, Russia

[2]Shubnikov Institute of Crystallography, Federal Scientific Research Centre "Crystallography and Photonics", Russian Academy of Sciences, Leninsky Avenue 59, Moscow, 119333 Russia

[3]Institute of Problems of Chemical Physics, Russian Academy of Sciences, Chernogolovka, Moscow region, 142432, Russia

[4]Faculty of Geology, Moscow State University, Vorobievy Gory, 119991 Moscow, Russia

[5]Institute of the Earth's Crust, Siberian Branch of Russian Academy of Sciences, Lermontova Street 128, Irkutsk, 664033, Russia

ABSTRACT

The new sodalite-group mineral species slyudyankaite, ideally $Na_{28}Ca_4(Si_{24}Al_{24}O_{96})(SO_4)_6(S_6)_{1/3}(CO_2)\cdot 2H_2O$, was discovered in altered lazurite-bearing metasomatic rock at the Malo-Bystrinskoe gem lazurite deposit, Baikal Lake area, eastern Siberia, Russia. The associated minerals are diopside, calcite, fluorapatite, phlogopite, lazurite, and pyrite. Slyudyankaite forms green to pale blue isolated anhedral equant grains up to 0.5 cm

across and their aggregates. The streak is white and the lustre is vitreous. Slyudyankaite is brittle, with a Mohs hardness of 5½. Cleavage and parting are not observed. Density measured by flotation in heavy liquids is equal to 2.46(2) $g \cdot cm^{-3}$. Density calculated using the empirical formula and unit-cell volume refined from single-crystal XRD data is 2.454 $g \cdot cm^{-3}$. Slyudyankaite was characterized using the IR, Raman, ESR, near infrared (NIR), visible (Vis) and ultraviolet (UV) absorption, XPS and photoluminescence spectroscopy methods. The chemical composition is (wt.%, electron microprobe, H_2O and CO_2 determined by selective sorption of ignition products, CO_2 confirmed by quantitative IR spectroscopic method, sulfate sulfur determined by wet chemical analysis): Na_2O 19.28, K_2O 0.12, CaO 5.13, Al_2O_3 27.01, SiO_2 33.25, SO_3 10.94, S 1.75, Cl 0.10, CO_2 1.42, H_2O 0.90, –O≡(Cl,HS) –0.03, total 99.87. The empirical formula is $Na_{27.57}Ca_{4.05}K_{0.11}(Si_{24.52}Al_{23.48}O_{96})(SO_4)_{6.06}S^0_{2.42}Cl_{0.12}(CO_2)_{1.43} \cdot 2.21H_2O$ where $S^0_{2.42}$ is the total sulfide sulfur, mainly occurring as neutral S_6 and subordinate S_4 molecules, according to the structural data. XPS spectroscopy confirms the presence of sulfide sulfur in neutral form. The crystal structure was determined using single-crystal X-ray diffraction data and refined to $R = 0.0428$. Slyudyankaite is triclinic, space group $P1$, $a = 9.0523$ (4) Å, $b = 12.8806$ (6) Å, $c = 25.681$ (1) Å, $\alpha = 89.988(2)°$, $\beta = 90.052(1)°$, $\gamma = 90.221(1)°$, $V = 2994.4$ (2) $Å^3$, $Z = 1$. Slyudyankaite contains two kinds of sodalite cages occurring in the structure in a ratio of 3:1. Cages of the first kind are completely occupied by SO_4^{2-} anions and extra-framework cations whereas cages of the second type contain only neutral molecules (S_6, CO_2, H_2O, and minor S_4). The strongest lines of the powder X-ray diffraction pattern [*d,* Å (*I*, %) (*hkl*)] are: 6.45 (11) (004, 112, 020), 3.716 (100) (204, 220, 116, 132), 2.878 (12) (136, 028, 044), 2.625 (23) (208, 240), 2.431 (6) (209), 2.275 (6) (048), 2.143 (12) (0.0.12, 336), 1,784 (7) (444, 1.1.14, 356, 172).

Keywords: Slyudyankaite, sodalite group, microporous materials, polysulfide groups, crystal structure, X-ray diffraction, spectroscopy

INTRODUCTION

The new mineral species slyudyankaite, $Na_{28}Ca_4(Si_{24}Al_{24}O_{96})(SO_4)_6(S_6)_{1/3}(CO_2)\cdot 2H_2O$, considered ~~described~~ in this paper, was earlier described as "triclinic lazurite" (Ivanov and Sapozhnikov, 1985; ICDD card 041-1392). Based on new data on the chemical composition, spectroscopic characteristics and crystal structure refinement, it has been shown that "triclinic lazurite" is a new sodalite-group mineral with alternating sodalite cages of two kinds. Cages of the first kind are occupied by extra-framework cations and anions whereas cages of the second kind contain only neutral molecules (S_6, CO_2, H_2O, and minor S_4).

The new mineral and its name have been approved by the IMA CNMNC (IMA No. 2021-062a). The type material is deposited in the collection of the Sidorov Mineralogical Museum (INRTU), Irkutsk, Russia with the registration numbers MMU/MF 27296 (holotype) and MMU/MF 27297 (cotype).

GEOLOGICAL SETTING AND PETROLOGICAL DATA

The rocks of the lazurite deposits of the Baikal region were formed during three stages of a single process of petrogenesis (Korzhinsky 1947, Ivanov and Sapozhnikov 1985). The earliest was the stage of regional metamorphism, which took place under the conditions of the granulite facies or the upper steps of the amphibolite facies. Metamorphic rocks are represented by marbles (primarily, dolomite ones), less often schists. The second (magmatic) stage was characterized by transformations of the metamorphic rocks and appearance of skarns, calciphyres and metasomatic aluminosilicate rocks. Within the limits of the lazurite deposits, the main role is played by leucocratic (mainly, composed of feldspars, quartz, and feldspathoids) magmatic granitoids, which compose concordant lenticular bodies, veins and stock-like bodies. Dolomite marbles have a noticeable effect on the magma composition. Depending on local

conditions, syenites, nepheline syenites, or anorthosites were formed. These rocks are usually endocontact facies of granitoids, but they can also be observed as independent vein-shaped bodies.

The overwhelming majority of lazurite-bearing rocks were formed at the postmagmatic stage following the stage at which plagioclase was substituted by feldspathoids. At the latter stage, granitoids were substituted by a rock mainly composed of potassium feldspar, with diopside, and calcite as subordinate components. However, at the contacts with alkaline rocks (nepheline syenites) and skarns this rock is absent. At the latest postmagmatic stage, hydrothermal processes resulting in the crystallization of scapolite, phlogopite, native sulfur and zeolites took place.

At the contact of granites with dolomite marbles, the following bimetasomatic zoning is observed: rock of syenite composition → diopside-lazurite rocks → lapis lazuli calciphyre → recrystallized and calcitized marble. The first two zones develop at the expense of granites, and the other ones were formed substituting dolomite marble. Lazurite and lazurite-related sodalite-group minerals containing sulfide sulfur are associated with diopside, calcite, dolomite, fluorapatite, phlogopite, pyrite and/or pyrrhotite, and graphite. The ratios of the contents of the main rock-forming components (sodalite-group minerals and diopside) are variable. Rocks substituting nepheline syenite are most enriched in lazurite and lazurite-related minerals.

Zones of lazurite calciphyres (*i.e*. calcite-dominant rocks composed of the same minerals as diopside-lazurite rocks) were formed as a result of infiltration metasomatism. Some of these rocks contain rather large (up to 20 mm across) crystals of lazurite and related minerals. The formation of lazurite calciphyres was accompanied by recrystallization and calcitization of the host dolomite marbles.

Locally, other metasomatic rocks (lazurite-orthoclase, lazurite-scapolite, lazurite-phlogopite, and lazurite-forsterite ones) are observed. At a high activity of Cl, rocks of the same facies containing afghanite instead of lazurite were formed. In the flanks of lazurite deposits,

diopside-phlogopite and phlogopite-calcite metasomatites are common. These rocks were formed in a low-alkaline magnesium-rich environment. In the calcareous environment, wollastonite metasomatites were formed.

TYPE MATERIAL: GENERAL APPEARANCE AND PHYSICAL PROPERTIES

Slyudyankaite occurs as isolated anhedral equant grains up to 0.5 cm across and their aggregates (Fig. 1). The associated minerals are diopside, calcite, fluorapatite, phlogopite, lazurite, and pyrite. The holotype sample is presented by the greenish-blue variety. The green variety which differs from the holotype by the contents of trace chromophore components was investigated for comparison. The streak is white and the lustre is vitreous. Fluorescence is not observed.

Slyudyankaite is brittle, and its Mohs hardness is 5½. Cleavage and parting are not observed. The fracture is uneven. Density measured by flotation in heavy liquids (bromoform + heptane) is equal to 2.46(2) $g \cdot cm^{-3}$. Density calculated using the empirical formula and unit-cell volume refined from single-crystal XRD data is 2.454 $g \cdot cm^{-3}$.

FIGURE 1. Slyudyankaite: (a) grains (bluish green to pale blue) in metasomatic rock with lazurite (dark blue), calcite (white), and pyrite (yellow), and (b) a fragment of holotype. The FOV widths are (a) 1.5 cm and (b) 0.8 mm.

EXPERIMENTAL METHODS

Infrared spectroscopy

This is the peer-reviewed, final accepted version for American Mineralogist, published by the Mineralogical Society of America.
The published version is subject to change. Cite as Authors (Year) Title. American Mineralogist, in press.
DOI: https://doi.org/10.2138/am-2022-8598. http://www.minsocam.org/

IR absorption spectra of slyudyankaite and other S-bearing sodalite-group minerals (used for comparison) were obtained using an ALPHA FTIR spectrometer (Bruker Optics) at a resolution of 4 cm^{-1}. The powdered samples were mixed with anhydrous KBr and pelletized. A total of 16 scans were collected for each spectrum. The IR spectrum of an analogous pellet of pure KBr was used as a reference.

Raman spectroscopy

Raman spectra of randomly oriented grains of slyudyankaite and other sodalite-group minerals used for comparison were obtained at room temperature using an EnSpectr R532 spectrometer based on an OLYMPUS CX 41 microscope coupled with a diode laser (λ = 532 nm). The spectra were recorded in the range from 100 to 4000 cm^{-1} with a diffraction grating (1800 gr mm^{-1}) and spectral resolution about 6 cm^{-1}. The output power of the laser beam was in the range from 5 to 13 mW. The diameter of the focal spot on the sample was 5 – 10 μm. The backscattered Raman signal was collected with a 40× objective; signal acquisition time for a single scan of the spectral range was 1 s, and the signal was averaged over 50 scans. Crystalline silicon was used as a standard.

ESR spectroscopy

ESR measurements were performed in the X-band (9.358 GHz) with a RE-1306 spectrometer (KBST, Smolensk, Russia) at the temperature of 296 K. To obtain ESR spectrum, small randomly oriented crystals of slyudyankaite were placed in a silica-glass test tube.

Optical UV–Vis–near IR absorption spectroscopy

Diffuse-light optical absorption spectra of slyudyankaite were recorded at room temperature with a commercial Perkin-Elmer Lambda 950 spectrophotometer (Perkin-Elmer, Shelton, CT, USA) in an integrating sphere. For measurements, the samples were placed in a

silica-glass test tube, which is transparent in the range of 285–2000 nm (35000 – 5000 cm^{-1}). The light beam was completely concentrated on the sample.

The photoluminescence spectra were measured under 405 nm laser excitation. The luminescence signal was recorded by a SDL-1 double grating monochromator (LOMO, St. Petersburg, Russia) and a Hamamatsu H6780-04 photomodule (185–850 nm) operating in the photon counting regime. A spectral slit width was about 0.05 nm. The measurements at 77 K were performed in a flooded nitrogen cryostat. To obtain photoluminescence spectra, a small single crystal of slyudyankaite was attached to a cryofinger and the temperature was recorded using a type-K thermocouple.

X-ray photoelectron spectroscopy

X-ray photoelectron spectra (XPS) were obtained with a SPECS instrument (SPECS, Germany) equipped with a PHOIBOS 150 MCD-9 electron energy analyzer at the Krasnoyarsk regional Centre for Collective Use, Siberian Branch of the Russian Academy of Sciences. The spectra were acquired at excitation initiated by monochromated Al$K\alpha$ (1486.74 eV) radiation. The high-resolution spectrum of S 2p (narrow scan) was recorded with a 0.05 eV interval and a transmission energy of 8 eV. The slyudyankaite sample was powdered to a mean particle size of 0.01 – 0.02 mm immediately before placing in the analysis chamber. The surface charging typical for dielectrics was eliminated using low-energy electron gun. The C 1s peak at 285 eV from natural hydrocarbon contaminants was used to correct the binding energies (BE) for the surface charging. The 2p sulfur spin-orbital doublet was unfolded and fitted by CasaXPS software after subtracting the nonlinear background by Shirley's method and taking into account separation of the doublet components S $2p_{3/2}$ and S $2p_{1/2}$ equal to 1.2 eV and the proportion of their intensities as 2:1. The peak shapes were described by the Voigt function (i.e., convolution of the Gauss and Lorentz functions). Peak attribution was performed according to data published previously (Tauson et al. 2012). The accuracy of the BE was estimated to be ±0.1 eV.

Optical measurements

Optical properties were determined for a powder sample using light with a wavelength of 589 nm.

Chemical composition

The samples of slyudyankaite were analyzed on a JXA–8200 Jeol electron microprobe equipped with a high-resolution scanning electron microscope, an energy dispersion system (EDS), a SiLi detector with a resolution of 133 eV, and five wave dispersion spectrometers (WDS). The chemical composition was measured with WDS operated at an acceleration voltage of 20 kV, with a current intensity of 10 nA and a counting time of 10 s. The beam was defocused to 20 μm to decrease the thermal effect on the sample. Under these conditions, the mineral was stable with respect to the electron beam influence.

The following standards and analytical lines were used: pyrope (Si, Kα), albite (Al, Na, Kα), diopside (Ca, Kα), orthoclase (K, Kα), barite (S, Kα), and Cl-apatite (Cl, Kα). The elemental contents were calculated using the ZAF procedure. Seven spot analyses were obtained. The back-scattered images did not reveal sulfide inclusions.

Electron microprobe analysis (EMPA) was used to determine the total sulfur content in the samples. Sulfate sulfur was determined by conventional wet chemical analysis using acidic decomposition. The content of sulfide sulfur was calculated as the difference between the total sulfur and the sulfate sulfur.

H_2O was determined using a modified Penfield method based on selective sorption of H_2O on $Mg(ClO_4)_2$ from gaseous products obtained by heating the mineral in oxygen at 1080°C.

For the determination of CO_2, two independent methods were applied. Selective sorption of CO_2 carried out on *askarite* sorbent (an asbestiform matter saturated by NaOH) from gaseous products obtained by heating the mineral at 1080°C in oxygen at 1 atm gave a CO_2 content of

1.46 wt%. Another method, which is based on determination of the intensity of the band at 2341 cm^{-1} in the IR spectrum (Chukanov et al. 2020a), resulted in a CO_2 content of 1.42 wt%. As the former value may include CO_2 in microscopic calcite inclusions, the latter value may be more reliable.

X-ray diffraction

Powder X-ray diffraction experiment was carried out at room temperature with an automatic powder diffractometer (D8 ADVANCE, Bruker, Germany) equipped with a Göbel mirror. Powder X-ray diffraction patterns were obtained in step scan mode (in the 2θ range from 5 to 80°), using Cu*K*α radiation, at an accelerating voltage of 40 kV, current of 40 mA, time per step of 1 s, and 2θ step of 0.02°. Calculations of interplanar distances and intensities of diffraction lines were performed using the DIFFRAC Plus software (Evaluation package EVA, Bruker AXS).

Single-crystal X-ray diffraction analysis of slyudyankaite was carried out using a Bruker AXS D8 Venture automated diffractometer (Bruker, Berlin, Germany) at the Favorsky Institute of Chemistry, Siberian Branch of the Russian Academy of Sciences (Irkutsk, Russian Federation). The X-ray data were acquired using a graphite monochromatized Mo*K*α radiation and a Photon 100 detector. Diffraction data were collected at 170 K using a Bruker Cobra nitrogen cryostat (Bruker, Berlin, Germany), at an operating voltage of 50 kV, current of 1 mA, and crystal-to-detector distance of 40 mm. The collection strategy was optimized by the COSMO program in the APEX2 suite package (Bruker 2007a). The X-ray data were collected in a complete sphere of the reciprocal space ($\pm h$, $\pm k$, $\pm l$) up to θ_{max} ~40° by a combination of several ω and ϕ rotation sets, with a scan step of 0.5° and exposure time of 6 s per frame. The reflection intensities were extracted and corrected for Lorentz factor and polarization using the SAINT package (Bruker 2007b). A semi-empirical absorption correction was applied by means of the

SADABS software (Sheldrick 2003). The XPREP software (Sheldrick 2008) was employed for determination of the space group and processing of the intensity statistics.

Data on the single-crystal experiment and crystal structure refinement are given in Table 1.

RESULTS AND DISCUSSION

Infrared spectroscopy

The assignment of absorption bands in the IR spectrum of slyudyankaite (Fig. 2) based on data from Steudel (2003), Eckert and Steudel (2003), Steudel and Chivers (2019), Rejmak (2020), Chukanov et al. (2020a,b), and Sapozhnikov et al. (2021a) is as follows.

3380 to 3610 cm^{-1} – O–H stretching vibrations (hydrogen bonds of medium strengths).

3240 cm^{-1} (shoulder) – O–H stretching vibrations (strong hydrogen bond or strong dipole-dipole interactions with CO_2 molecules).

2385 cm^{-1} (weak band) – presumably, antisymmetric stretching vibrations of $^{12}CO_2$ molecules which are acceptors of strong hydrogen bonds.

2341 cm^{-1} – antisymmetric stretching vibrations of the major part of $^{12}CO_2$ molecules.

2275 cm^{-1} – antisymmetric stretching vibrations of the $^{13}CO_2$ molecules.

2040 cm^{-1} (very weak band) – C–O stretching vibrations of trace admixture of the O=C=S molecules which are common in samples containing both sulfide sulfur and CO_2 (Tubergen et al. 2000, Chukanov et al. 2020a,b).

1632 cm^{-1} – bending vibrations of the H_2O molecules (an indistinct shoulder at ~1680 cm^{-1} may correspond to H_2O molecules forming strong hydrogen bonds).

1138 and 1107 cm^{-1} – asymmetric stretching vibrations of the SO_4^{2-} anionic groups (the degenerate $F_2(\nu_3)$ mode).

1002 cm^{-1} – stretching vibrations of the aluminosilicate framework.

This is the peer-reviewed, final accepted version for American Mineralogist, published by the Mineralogical Society of America.
The published version is subject to change. Cite as Authors (Year) Title. American Mineralogist, in press.
DOI: https://doi.org/10.2138/am-2022-8598. http://www.minsocam.org/

The range of 650–720 cm^{-1} – mixed vibrations of the aluminosilicate framework.

641 cm^{-1} – stretching vibrations of the neutral S_4 molecule having cis conformation (Rejmak, 2020; see structural data below). This band is absent in other sodalite-group and sodalite-related minerals.

614 cm^{-1} – bending vibrations of the SO_4^{2-} anionic groups (the degenerate $F_2(v_4)$ mode). Analogous bands of SO_4^{2-}-bearing sodalite-group minerals are observed in the range of 612 – 625 cm^{-1} and are absent in the IR spectra of sulfate-free members of the sodalite group, i.e. sodalite and its HS^--dominant analogue sapozhnikovite $Na_8(Al_6Si_6O_{24})(HS)_2$, (Chukanov et al. 2022a).

Below 550 cm^{-1} – mainly, lattice modes involving bending vibrations of the aluminosilicate framework and libration vibrations of SO_4^{2-} and extra-framework molecules. A shoulder at ~465 cm^{-1} may be partly due to stretching vibrations of cyclic S_6 molecule having D_{3d} symmetry (Eckert and Steudel 2003).

FIGURE 2. Powder infrared absorption spectra of (*a*) slyudyankaite, (*b*) haüyne $(Na_{5.52}K_{0.35}Ca_{1.99})(Si_{6.10}Al_{5.81}Fe^{3+}_{0.09}O_{24})(SO_4)_{1.97}Cl_{0.11}\cdot nH_2O$ (Chukanov et al. 2020b) from the Laach Lake volcano, Eifel paleovolcanic region, Germany, and (*c*) lazurite neotype sample $(Na_{6.97}Ca_{0.88}K_{0.10})(Al_{5.96}Si_{6.04}O_{24})(SO_4^{2-})_{1.09}(S_3^{\bullet-})_{0.55}S^{2-}_{0.05}Cl_{0.04}\cdot 0.72H_2O$ from the Malo-Bystrinskoe deposit, Baikal Lake area. In the inset, IR spectrum of slyudyankaite in the range of 1500 – 3800 cm^{-1} is shown. The spectra are offset for comparison.

The integral intensity of the bands of asymmetric stretching vibrations of the SO_4^{2-} anionic groups correlates with the total content of these groups which occupy 50%, 75% and 100% of sodalite cages in lazurite, slyudyankaite and haüyne, respectively (Fig. 2).

The bands at 3240 and 2385 cm^{-1} may correspond to donor and acceptor of the same strong hydrogen bond (H_2O and CO_2 molecules, respectively), but the fractions of such molecules among the totality of H_2O and CO_2 are low.

Bands of CO_3^{2-} anions (in the range of 1350 – 1550 cm^{-1}) and $S_3^{\bullet-}$ radical anions (at ~580 cm^{-1}: Chukanov et al. 2020a,b; Sapozhnikov et al. 2021a) are not observed in the IR spectrum of slyudyankaite.

Raman spectroscopy

The assignment of Raman bands of slyudyankaite (Fig. 3) given in Table 2 is based on data from Steudel (2003), Eckert and Steudel (2003), Ling et al. (2011), Steudel and Chivers (2019), Wong and Steudel, 2003; Rejmak (2020), Chukanov et al. (2020a,b), and Sapozhnikov et al. (2021a).

FIGURE 3. Raman spectrum of the slyudyankaite holotype sample.

The Raman spectrum of slyudyankaite differs significantly from the spectra of different varieties of another Ca- and SO_4-bearing sodalite-related mineral, haüyne (Fig. 1S). Non-cyclic polysulfide species are strong Raman scatterers (Rejmak 2020; Chukanov et al. 2020a,b). As a result, in the Raman spectrum of slyudyankaite, numerous bands of S_4 and $S_3^{\bullet-}$ are observed despite these species occur in the mineral in very low amounts (see below for details). The most significant specific feature of the Raman spectrum of slyudyankaite is the presence of bands corresponding to the S_4 and S_6 neutral molecules.

FIGURE 1S. Raman spectra of (*a*) blue haüyne $(Na_{5.52}K_{0.35}Ca_{1.99})(Si_{6.10}Al_{5.81}Fe^{3+}_{0.09}O_{24})(SO_4)_{1.97}Cl_{0.11}\cdot nH_2O$ with trace amounts of the $S_3^{\bullet-}$ chromophore from the Laach Lake volcano, Eifel paleovolcanic region, Germany, and (*b*) lilac sulfide-bearing haüyne $(Na_{6.45}Ca_{1.36}K_{0.01})(Al_{5.94}Si_{6.06}O_{24})(SO_4)_{1.56}(S_4)_{0.09}(S_3^{\bullet-})_{0.035}Cl_{0.09}\cdot nH_2O$ containing both red (S_4) and blue ($S_3^{\bullet-}$) chromophores from the Malo-Bystrinskoe deposit, Baikal Lake area (Chukanov et al. 2020b).

This is the peer-reviewed, final accepted version for American Mineralogist, published by the Mineralogical Society of America.
The published version is subject to change. Cite as Authors (Year) Title. American Mineralogist, in press.
DOI: https://doi.org/10.2138/am-2022-8598. http://www.minsocam.org/

Bands of CO_3^{2-} anions are not observed in the Raman spectrum of slyudyankaite. Thus, all carbon in this mineral belongs to neutral CO_2 molecules, which is in agreement with the IR spectrum of slyudyankaite.

The extinction coefficients of IR bands of S–H stretching vibrations are very small (Sheppard 1949, Bragin et al. 1977). Raman spectroscopy is very sensitive to such modes (see *e.g.* Fig. 2S). However, the intensity of the Raman band at 2575 cm^{-1} is low. Thus, the S–H bearing species occurs in slyudyankaite in trace amounts.

FIGURE 2S. Infrared (***a***) and Raman (***b***) spectra of polycrystalline ammonium hydrosulfide $(NH_4)(HS)$ drawn using data from Bragin et al. (1977). The band at 2565 cm^{-1} corresponds to stretching vibrations of the HS^- anion.

The Raman shift of the narrow and very strong band corresponding to S–H stretching vibrations is observed at 2553 cm^{-1} for the HS^- anion in the sodalite cage of sapozhnikovite (Chukanov et al. 2022a) and at 2565 cm^{-1} for HS^- in $(NH_4)(HS)$ (Bragin et al. 1977). Thus, the weak and narrow band at 2575 cm^{-1} in the Raman spectrum of slyudyankaite may correspond to trace amounts of HS^-.

ESR spectroscopy

The electron spin resonance (ESR) spectrum of slyudyankaite is shown in Fig. 4. A strong signal with g-factor of 2.030 corresponding to the $S_3^{\bullet-}$ radical anion (Sapozhnikov et al. 2021a) is observed.

FIGURE 4. ESR spectrum (first derivative) of the slyudyankaite holotype sample. The inset shows the dependence of the $S_3^{\bullet-}$ content in sodalite-group minerals (after Chukanov et al. 2020b – triangles) on measured doubly integrated ESR signal intensity obtained under similar conditions. The circle corresponds to slyudyankaite.

This is the peer-reviewed, final accepted version for American Mineralogist, published by the Mineralogical Society of America.
The published version is subject to change. Cite as Authors (Year) Title. American Mineralogist, in press.
DOI: https://doi.org/10.2138/am-2022-8598. http://www.minsocam.org/

In order to estimate the content of $S_3^{\bullet-}$ in slyudyankaite, the intensity of its integrated ESR signal was compared with those in the ESR spectra of sodalite-group minerals with known $S_3^{\bullet-}$ contents (Chukanov et al. 2020b). As shown in Fig. 4, the intensity of the $S_3^{\bullet-}$ signal in the ESR spectrum of slyudyankaite corresponds to an extrapolated $S_3^{\bullet-}$ content below 0.01 radical anions per formula unit with $(Si,Al)_{12}$. Such low content of $S_3^{\bullet-}$ could not be detected by means of X-ray structural analysis, but the presence of this very strong blue chromophore along with S_6 (a yellow chromophore) in slyudyankaite is important for understanding the nature of green to greenish-blue color of this mineral. Apparently, at high concentrations of the $S_3^{\bullet-}$ radical anions, the ESR signal is saturated, and the dependence of the ESR signal intensity on the concentration becomes nonlinear. Previously, a similar saturation of the ESR signal in samples with high concentrations of $S_3^{\bullet-}$ was observed by Wujcik et al. (2016). However, at $S_3^{\bullet-}$ concentrations less than 0.1 per formula unit, the linear correlation between the integrated intensity of the ESR signal and the radical anion concentration is preserved.

UV–Vis–near IR absorption spectroscopy

Diffuse-light optical absorption spectra of slyudyankaite in the NIR, visible and near UV ranges are given in Fig. 5.

FIGURE 5. UV–Vis–near IR absorption spectra of (*a*) slyudyankaite holotype (greenish-blue) sample and (*b*) green slyudyankaite variety.

Two samples (both triclinic, with slyudyankaite-type unit-cell parameters) were investigated. Curve *a* in Fig. 5 corresponds to the holotype sample which has a somewhat dull greenish-blue color, and curve *b* corresponds to a bright green slyudyankaite variety from the association with slyudyankaite holotype. In both spectra, absorption in the range of 450 – 700 nm is a combination of bands from several color centers. One of them (at ~610 nm) is due to the

This is the peer-reviewed, final accepted version for American Mineralogist, published by the Mineralogical Society of America.
The published version is subject to change. Cite as Authors (Year) Title. American Mineralogist, in press.
DOI: https://doi.org/10.2138/am-2022-8598. http://www.minsocam.org/

presence of $S_3^{\bullet-}$ radical anions (Chukanov et al. 2020b; see ESR spectroscopy data). Another one (at ~530–540 nm) may correspond to neutral S_4 molecules having *cis*-conformation (Weser et al. 1978, Eckert and Steudel 2003; Paniz and Lester 1992). In addition, the presence of *trans*-S_4 molecules absorbing at ~625 nm (Eckert and Steudel, 2003) is not excluded.

A broad absorption band located at 580 nm was observed in the visible spectrum of the oxidized species S_4N^- (Dubois et al. 1989). Therefore, the lower wavelength part of the plateau in the region 500 – 700 nm may be tentatively assigned to the contribution of S_4H^-. This assumption is in agreement with the band of S–H stretching vibrations observed in the Raman spectrum of slyudyankaite at 2575 cm^{-1}.

In the range of 350 – 450 nm, structure-less absorption is observed for the green slyudyankaite variety. In this spectral region, $S_2^{\bullet-}$ radical anion absorbs, which can be detected by characteristic photoluminescence (see below). However, in the holotype sample of slyudyankaite (in contrast to the green variety of this mineral), photoluminescence was not detected even at a maximum slit width, which allows us to conclude that such anions are absent in the holotype.

Absorption in the range of 350 – 450 nm can also be associated with the presence of the S_4^{2-} (Billmers and Smith 1991, Dubois et al., 1989, Steudel and Chivers 2019) or S_6^{2-} (the bands at 350 and 474 nm: Steudel and Chivers 2019). However, considering the charge balance requirement, negatively charged forms of sulfide sulfur are present in slyudyankaite in insignificant amounts.

S_4 molecule is a red chromophore. In the holotype slyudyankaite sample, red color is masked by the $S_3^{\bullet-}$ radical anion which is a strong blue chromophore. However, in the associated green slyudyankaite with a very low $S_3^{\bullet-}$ content (below the detection limit of UV–Vis–near IR absorption spectroscopy), red and yellow zones are observed (Fig. 6). Yellow color may be due to both S_6 and $S_2^{\bullet-}$. Luminescence spectrum confirms the presence of the $S_2^{\bullet-}$ radical anions in the green slyudyankaite variety (see below).

FIGURE 6. Fragment of a peripheral part of a green slyudyankaite grain. FOV width 150 μm.

Absorption below 400 nm may be partly related to the presence of S_6 molecules (Steudel et al. 1988; Steudel and Chivers 2019, Tossel, 2003).

Photoluminescence spectroscopy

As noted above, in the holotype sample of slyudyankaite photoluminescence was not detected. However, green slyudyankaite exhibits luminescence upon laser excitation at a wavelength of 405 nm (Fig. 7). The photoluminescence spectrum of the green variety was obtained at 77 K. Two bands were observed in the spectrum. The band at 665 nm having well-resolved vibrational structure corresponds to the $S_2^{\bullet-}$ radical anion (Kirk et al. 1965). The origin of second band at 520 nm is unclear. This band could be tentatively assigned to oxygen radical anion $O_2^{\bullet-}$ (Norrbo et al., 2015, 2016).

FIGURE 7. Emission spectrum of green slyudyankaite under 405 nm excitation at 77 K.

X-ray photoelectron spectroscopy

Figure 8 shows the narrow X-ray photoelectron spectrum of slyudyankaite. The following parameters for sulfur species are obtained: BE $2p_{3/2}$ = 164.0 and $2p_{1/2}$ = 165.2 eV for S^0; BE $2p_{3/2}$ = 167.9 and $2p_{1/2}$ = 169.1 eV for S(VI). Thus, the XPS data confirm the presence of sulfide sulfur in slyudyankaite in neutral form.

FIGURE 8. The S 2p XPS spectrum of slyudyankaite.

This is the peer-reviewed, final accepted version for American Mineralogist, published by the Mineralogical Society of America.
The published version is subject to change. Cite as Authors (Year) Title. American Mineralogist, in press.
DOI: https://doi.org/10.2138/am-2022-8598. http://www.minsocam.org/

Optical data

Slyudyankaite is optically biaxial (+) with $\alpha = 1.506(1)$, $\beta = 1.509(1)$, and $\gamma = 1.513(1)$ ($\lambda = 589$ nm). $2V$ (meas.) = 80(10)°, $2V$ (calc.) = 82°. Dispersion of optical axes is distinct. Orientation could not be determined because of the absence of cleavage and crystal forms.

Pleochroism is strong. The pleochroism scheme is X (colorless) < Y (green) < Z (greenish-blue).

Chemical composition and formula

Analytical data for slyudyankaite are given in Table 3. Contents of other elements with atomic numbers larger than that of beryllium are below the detection limits. Oxygen equivalent for S was not introduced because, according to structural and spectroscopic data, almost all sulfide sulfur belongs to neutral molecules.

The empirical formula based on 48 Al + Si atoms per formula unit ($Z = 1$) is $Na_{27.57}Ca_{4.05}K_{0.11}(Si_{24.52}Al_{23.48}O_{96})(SO_4)_{6.06}S^0_{2.42}Cl_{0.12}(CO_2)_{1.43}\cdot 2.21H_2O$ where $S^0_{2.42}$ is the total sulfide sulfur, mainly occurring as neutral S_6 and subordinate S_4 molecules, according to the structural data (see below). This formula has an excessive negative charge of –0.06 which may be due to the presence of trace admixtures of $S_3^{\bullet-}$ and $S_4^{\bullet-}$ radical anions detected by sensitive ESR and Raman spectroscopy.

Taking into account structural data (see below), the simplified formula can be written as follows: $(Na,K,Ca)_{28}Ca_4[Si_{24}(Al,Si)_{24}O_{96}](SO_4)_6[(S_6,S_4)_x(CO_2)_y]\cdot 2H_2O$ ($\frac{1}{3} \le x \le 0.5$, $1 \le y \le 1.5$, $x + y \le 2$). The ideal formula of slyudyankaite is $Na_{28}Ca_4(Si_{24}Al_{24}O_{96})(SO_4)_6S^0_2(CO_2)\cdot 2H_2O$ (with S^0 being total sulfide sulfur belonging to neutral molecules, such as S_6 and S_4 with the predominance of S_6), or $Na_{28}Ca_4(Si_{24}Al_{24}O_{96})(SO_4)_6(S_6)_{1/3}(CO_2)\cdot 2H_2O$, which requires Na_2O 19.80, CaO 5.12, Al_2O_3 27.91, SiO_2 32.90, SO_3 10.96, S 1.46, CO_2 1.05, H_2O 0.82, total 100 wt.%.

X-ray diffraction

Powder X-ray diffraction data for slyudyankaite are given in Table 4. Based on single-crystal data (see below), the mineral is triclinic. In general, a triclinic unit cell is characterized by nonequivalent linear parameters ($a \neq b \neq c$) and angles ($\alpha \neq \beta \neq \gamma$). In the reciprocal space of a triclinic lattice, there are groups of eight reflections, nonequivalent in position and intensity, with *hkl* indices which are identical in absolute values but differ from each other by the signs: *hkl*, -*hkl*, *h-kl*, *hk-l*, *h-k-l*, *-h-k,l*, *-hk-l*, and *-h-k-l*. In the orthogonal unit cell with $\alpha = \beta = \gamma = 90°$, *d* values of these reflections are identical. In the pseudo-orthorhombic unit cell of slyudyankaite, deviations of α, β, and γ angles from 90° are very small, and related reflections with different signs of indices cannot be observed separately due to their overlapping. Moreover, in the powder X-ray diffraction pattern some groups of close reflections (002 and 010; 100 and 012; 102 and 110; 111 and 013; 004 and 112; 114 and 122; 200 and 024; 115 and 211; 212, 124, and 016; 203 and 035; 204, 220, 116, and 132; etc.) are observed as single broadened peaks. For this reason, only indices with positive *h*, *k*, and *l* values and minimum $h + k + l$ sums are indicated in Table 4.

As a result of the overlapping of individual reflections, peaks observed in the powder X-ray diffraction pattern of slyudyankaite are broadened as compared to those of cubic lazurite (Fig. 9). The ratios of half-widths for the peaks a, b, c, and d of slyudyankaite and cubic lazurite shown in Fig. 9 are equal to 1.44, 1.83, 1.59 and 1.32, respectively.

FIGURE 9. Comparison of the shapes of the diffraction peaks of slyudyankaite (black) and cubic lazurite with $a = 9.071$ Å (red). Lazurite peaks are marked with $(hkl)_{cub}$ indices. The interplanar distances *d* for the slyudyankaite peaks are indicated at the bottom (see Table 4).

This is the peer-reviewed, final accepted version for American Mineralogist, published by the Mineralogical Society of America.
The published version is subject to change. Cite as Authors (Year) Title. American Mineralogist, in press.
DOI: https://doi.org/10.2138/am-2022-8598. http://www.minsocam.org/

The room-temperature triclinic unit-cell parameters refined from the powder data are as follows: a = 9.094(7) Å, $b = a\sqrt{2}$ = 12.861(8) Å, $c = 2a\sqrt{2}$ = 25.722(15) Å, α = 90°, β = 90°, γ = 90°, V = 3008 (3) Å^3. The unit-cell parameters determined from the single-crystal data at 170 K are: a = 9.0523(4) Å, b = 12.8806(6) Å, c = 25.681 (1) Å, α = 89.988(2)°, β = 90.052(1)°, γ = 90.221(1)°, V = 2994.4(2) Å^3. Of the three angles, only the angle γ = 90.221(1)° noticeably differs from 90°, which suggests the monoclinic symmetry of the crystal. According to the results of the structure refinement (see tables of atomic coordinates in the Supplementary Materials), for most atoms with coordinates (x, y, z) it is possible to select a pair of the same sort near (x+½, y, –z), but the accuracy of the correspondence is often out of the margin of error. In addition, the monoclinic $P11a$ symmetry is obviously violated by the asymmetric distribution of the S_6 rings. A number of reflections (including those in the low-angle region, with the d values of 12.93, 11.49, 7.43, and 7.12 Å) cannot be indexed in the cubic sodalite-type unit cell that is an important diagnostic feature of slyudyankaite

The comparison of powder and single-crystal unit-cell parameters obtained at different temperatures shows that thermal expansion of slyudyankaite is significantly anisotropic. The thermal expansion coefficient of the unit-cell volume is equal to 0.107 Å^3·K^{-1} which corresponds to a bulk thermal expansion coefficient of $3.54 \cdot 10^{-5}$ K^{-1}.

Crystal structure

According to the results of structural analysis (see Fig. 10, Tables 5–9, 1S–4S), Na and Ca cations occupy a total of 32 sites in the unit cell, of which 24 sites (Na1 to Na24 in the list of coordinates) are occupied by Na atoms. The remaining 8 positions are mixed. Two of them, namely (Ca,Na)25 and (Ca,Na)27, are populated in the ratio of Ca:Na = 3:1 whereas the (Ca,Na)31 and (Ca,Na)32 sites are populated in the inverse proportion, Ca:Na = 1:3. The remaining four sites are populated with calcium and sodium in the ratio of Ca:Na = 1:1. The numbers 1 and 2 in the figures denote cages that do not contain SO_4 tetrahedra.

FIGURE 10. The crystal structure of slyudyankaite (general view in *ac* and *bc* projections). The unit cell is outlined. AlO_4 tetrahedra are blue-green, SiO_4 tetrahedra are orange, and SO_4 tetrahedra are yellow. The symbols 1 and 2 denote sodalite cages that do not contain SO_4^{2-} anions.

Six out of the eight sodalite cages contain SO_4 tetrahedra. An attempt to refine the populations of sulfate sulfur sites gives a result of 93 – 99%, without a significant decrease in the refinement *R*-factor, and the difference Fourier synthesis of the electron density does not reveal residual peaks in these cages. Taking into account the results of chemical analysis, there is almost 100% population of the six cages with SO_4 tetrahedra. For brevity, below a sodalite cage with a central S1 atom is called an S1-cage, and so on up to S6. It is easy to see that SO_4 tetrahedron is always oriented in such a way as to get situated closer to Ca^{2+} cations. Two vertices of a tetrahedron occurring in the S3 cage with an occupancy of 75% are located at short distances (2.62 and 2.27 Å) from the sites which are 75% occupied by calcium, whereas a tetrahedron in an alternative orientation derived from the first tetrahedron by turning around one of its edges exists with an occupancy of 25%. In the latter case, oxygen atoms in new sites at the ends of another edge are located at short distances from two other sites occupied by 25% with calcium. The S6 cage is populated with SO_4 tetrahedra in two equiprobable orientations and surrounded by calcium and sodium in the ratio Ca:Na = 1:1. In other words, the ratios of the amounts of sulfate groups with different orientations correlate with the Na:Ca ratio in adjacent sites.

Two remaining cages do not contain sulfate sulfur. An electron density map calculated by Fourier synthesis revealed that the first of the polysulfide species confidently seen in both cages is six-membered ring S_6 having a chair-like conformation (Figs. 11 and 12).

This is the peer-reviewed, final accepted version for American Mineralogist, published by the Mineralogical Society of America.
The published version is subject to change. Cite as Authors (Year) Title. American Mineralogist, in press.
DOI: https://doi.org/10.2138/am-2022-8598. http://www.minsocam.org/

FIGURE 11. Three nonequivalent S_6 molecules in sodalite cages (*bc* projection). The symbols 1 and 2 denote sodalite cages. Cages # 1 contains S_6 molecules in two orientations (a, b), while S_6 molecules in Cages # 2 are equally oriented (c).

FIGURE 12. Three nonequivalent S_6 molecules in the sodalite cages # 1 and # 2 (*ac* projection).

There are three 6-membered rings, one in cages #2 and two in cages #1. In each ring, atomic displacement parameters (ADPs) of the SS sites and the site occupancies were kept identical. In addition, it has been fixed that two rings in cages #1 exist with equal probability. After that, the structural parameters, including occupancies, of two SS sites, namely SS10 and SS20, were refined. About 12% of cages #2 are populated with identically oriented S_6 rings (Ss10–Ss11–Ss12–Ss13–Ss14–Ss15).

As can be seen from Figs. 10 to 12, cages #1 are populated with S_6 rings in two orientations, Ss20–Ss22–Ss23–Ss21–Ss24–Ss25 and Ss20–Ss26–Ss27–Ss21–Ss28–Ss29. The occupancies of cages #1 with two kinds of rings are equal to 22%. Thus, in total there are 0.34 S_6 units per unit cell of slyudyankaite, which is in good agreement with the chemical formula ($0.34 \times 6 = 2.04$ atoms of sulfide sulfur per formula unit). This result was obtained using the following procedure. Atomic displacement parameters (ADP) were set isotropic and equal to each other within the same ring. The populations of the sulfur positions were also set equal to each other within the same ring. In the cage #1, the populations of sites Ss20 and Ss21 common to two rings were doubled with respect to the populations of the remaining sites, *i.e*. the occupancies of sulfur sites in the two rings were set equal to 11% for each ring. All three rings have the chair conformation with the absolute values of the torsion angles between ~69 and ~79 degrees (see Table 7S).

The composition of $Na_{28}Ca_4(Al_6Si_6O_{24})_4(SO_4)_6$ is charge balanced. For this reason alone, it is reasonable to consider the S_6 atomic groups as neutral molecules rather than anionic groups.

This is the peer-reviewed, final accepted version for American Mineralogist, published by the Mineralogical Society of America.
The published version is subject to change. Cite as Authors (Year) Title. American Mineralogist, in press.
DOI: https://doi.org/10.2138/am-2022-8598. http://www.minsocam.org/

In addition, the S–S interatomic distances and the S–S–S angles (Table 11) are in good agreement with the theoretical estimates of these values in a neutral molecule S_6 (see *e.g.* Steidel et al. 1978, Jug and Iffert 1989). Distances between S atoms of the S_6 rings and nearest cations and O atoms of the framework are given in Tables 8 and 9.

Thus, only 22% of type 1 cavities and 12% of type 2 cavities are occupied by S_6 rings. The rest are either occupied by any other electrically neutral species, or are empty.

FIGURE 3S. Residual electron density distribution in slyudyankaite (3D visualization of the difference Fourier synthesis); $\Delta\rho(\text{min}) / \Delta\rho(\text{max}) = -1.69 / 2.38$ e Å^{-3}. Balls represent atoms from the structure model. See the text for further explanation.

At the next stage of the analysis, the Fourier synthesis of the electron density was carried out using the differences between $|F_{obs}|$ and $|F_{calc}|$ in a model containing framework atoms, Na^+ and Ca^{2+} cations, SO_4^{2-} anions, and S_6 molecules. The 3D image of the results of difference Fourier synthesis shown in Fig. 3S was obtained using the software VESTA (Momma and Izumi 2011). As one can see from the figure, the cages #1 and #2 are filled by "agglomerations" with positive electron density. In 2D sections of the maps of residual electron density, multiple weak (below 1.5 e Å^{-3}; mainly, below 1 e Å^{-3}) and partly diffuse maxima are observed. Based on the data on the chemical composition, we can conclude that most of the residual peaks correspond to CO_2 and H_2O molecules, as well as positions of sulfur atoms not taken into account in the model, with a population of no more than 3 – 5%. For comparison, the heights of the residual peaks for S_6 averaged 3.5 e Å^{-3}.

Thus, the chemical composition of slyudyankaite, determined from X-ray data, is in good agreement with the results of chemical analysis, if we neglect the locally small contributions of other polysulfides and other atomic groups (CO_2, H_2O and minor K and Cl).

This is the peer-reviewed, final accepted version for American Mineralogist, published by the Mineralogical Society of America.
The published version is subject to change. Cite as Authors (Year) Title. American Mineralogist, in press.
DOI: https://doi.org/10.2138/am-2022-8598. http://www.minsocam.org/

FIGURE 4S. Possible locations of (a) S4 and (b) S3 molecules in the sodalite cage # 2, in projection along the *a*-axis. Sulfur positions are numbered. In S4, interatomic distances 1–2, 2–3, 3–4, and 4–1 are equal to 2.08(1), 1.98(1), 1.98(1), and 2.53(1) Å, respectively; angles 1–2–3 and 2–3–4 are equal to 101.1(5) and 94.1(5)°, respectively. The 1–2–3–4 torsion angle equals to 1.4(6)°. In S3, interatomic distances 1–2 and 2–3 are equal to 1.93(1) and 1.91(1) Å, respectively and the 1–2–3 angle equals 115.6(6)°.

FIGURE 5S. Possible locations of (a) S4 and (b) S3 molecules in the sodalite cage #2, in projection along the b-axis.

Some of the H_2O and CO_2 molecules are connected by dipole-dipole interactions, comparable in energy with a strong hydrogen bond. These molecules correspond to the bands at 2385 and 3240 cm^{-1} in the IR spectrum and the band at 1340 cm^{-1} in the Raman spectrum. When a coupled pair of an H_2O molecule and a CO_2 molecule is placed in a sodalite cavity, the distance between the O atom of water and the C atom of the CO_2 molecule will presumably be 2.2 – 2.3 Å (Fig. 13). Several pairs with such distances can be selected among the residual peaks at the indicated distances, which is an argument in favor of this hypothesis.

FIGURE 13. Scheme of hypothetical mutual arrangement of H_2O and CO_2 molecules involved in strong dipole-dipole interactions.

DISCUSSION

The framework of topologically identical sodalite-related minerals (the **SOD**-type framework) is built involving three kinds of stacking of adjacent layers of Al- and Si-centered tetrahedra, *A*, *B,* and *C*, in the stacking sequence $(ABC)_\infty$ (Bonaccorsi and Merlino 2005; see also Database of Zeolite Structures, http://www.iza-structure.org/databases/). The layers contain six-membered rings of Si- and Al-centered tetrahedra which are ordered in most aluminosilicate sodalite-related minerals, including slyudyankaite.

This is the peer-reviewed, final accepted version for American Mineralogist, published by the Mineralogical Society of America.
The published version is subject to change. Cite as Authors (Year) Title. American Mineralogist, in press.
DOI: https://doi.org/10.2138/am-2022-8598. http://www.minsocam.org/

The stoichiometry of the framework of sulfate-bearing sodalite-group minerals is close to $AlSiO_4$. Extra-framework cations (mainly, Na^+, Ca^{2+}, and K^+), anions (SO_4^{2-}, S^{2-}, $S_2^{\bullet-}$, $S_3^{\bullet-}$, OH^-, F^-, HS^-, and Cl^-) as well as neutral molecules (H_2O, CO_2, S_4, S_6, and COS) occur in large cages in variable amounts (Chukanov et al. 2020a,b, 2022a; Sapozhnikov et al. 2021a,b). The **SOD**-type aluminosilicate framework contains 3D system of channels consisting of sodalite cages. Slyudyankaite has topologically the same aluminosilicate framework as other sodalite-group minerals. However, the framework of slyudyankaite is periodically distorted by structural modulations (Table 5). Earlier, this kind of modulation has been determined in "triclinic lazurite" (Evsyunin et al. 1997). The AlO_4 and SiO_4 tetrahedra in the slyudyankaite framework are shifted periodically along the *a* axis, and a modulation wave involving AlO_4 and SiO_4 tetrahedra with a period equal to the unit-cell parameter appears in the *c* axis direction. As a result, the shape and volume of the cavities of the framework periodically changes, which results in their population by different extra-framework components. The S–Na and S–O distances given in Tables 12 and 13 indicate a free placement of bulk S_6 rings in the largest cages which do not contain extra-framework ions. Figuratively speaking, the S_6 molecule, making room for itself, "pushes" the Na^+ and Ca^{2+} cations into the neighboring cages, where their positive charge is compensated by the SO_4^{2-} anions.

In cubic minerals of sodalite group, Si and Al are at partial sites with the coordinates (0.5, 0, 0.25) and (0.5, 0.25, 0) which are their ideal positions. In slyudyankaite, periodic displacements of atoms from their ideal positions in subcells (*i.e.* different semi-cells of the unit cell) lead to wave-like modulations of the structure. For Si and Al, the maximum deviation along the *a* axis is 0.458 Å whereas the displacement along the *b* axis is an order of magnitude smaller and amounts to 0.056 Å. A periodic displacement of sulfate sulfur atoms in the plane perpendicular to the c axis is also observed. The modulation wave propagates along the *c* axis and its period is equal to the unit-cell parameter. A distinguishing feature of slyudyankaite as an individual mineral species is the presence of two kinds of sodalite cages occurring in the

structure in the ratio of 3:1. Cages of the first kind are completely occupied by SO_4^{2-} anions and extra-framework cations whereas cages of the second type contain only neutral molecules (S_6, CO_2, H_2O, and minor S_4). The ordering of sulfate anions and neutral molecules occurring in the ratio of $SO_4 : S^0 : CO_2 : H_2O$ ratio of 6 : 2 : 1 : 2 (where S^0 is sulfide sulfur belonging to neutral molecules, predominantly S_6) defines slyudyankaite as a mineral species different from other sodalite-group minerals.

It was previously shown that triclinic sodalite-group minerals from the Malo-Bystrinskoe deposit contain polymerized neutral sulfur species S^0 (Tauson et al. 2012). The S^0 formation was interpreted as a result of polysulfide disproportionation $S_x^{2-} = (x - 1)S^{2-} + S^0$ or its interaction with thiosulfate in excess of oxygen: $S_x^{2-} + S_2O_3^{2-} + 2.5\ O_2 = x\ S^0 + 2\ SO_4^{2-}$. In accordance with the charge balance requirement, both reactions should be accompanied by electron transfer processes involving other extra-framework components. Thus, cubic lazurite and related members of the sodalite group from gem lazurite deposits represent high-temperature minerals crystallized at ~550 – 600 °C (Ivanov and Sapozhnikov, 1985) whereas their lower-symmetry analogues can form only at temperatures below 550 °C and, possibly, under more oxidizing conditions. The reason for this conclusion is that lower-symmetry lazurite analogues associate with cubic members of the lazurite-haüyne series with incommensurately 3D-modulated (ITM) structure "never heated in nature to more than 550 °C through the geologically meaningful time" (Tauson et al. 2014). This is in agreement with the general trend of lower symmetry of phases crystallized at relatively low temperatures as compared with their counterparts crystallized at higher temperatures.

The $S_3^{\bullet-}$ radical anion is one of the most stable polysulfide species at high temperatures (Steudel and Chivers, 2019). On the other hand, the SO_2 fugacity in ITM cubic lazurite stability field is relatively high (~10^{-5} to ~10^{-2} bar: Tauson et al. 1998) and this might cause instability of the $S_3^{\bullet-}$ species in solution and its dimerization to S_6 accompanied by electron transfer that is a well-known process in ultramarine synthesis (Clark et al. 1983). The annealing experiments with

triclinic lazurite demonstrated its complete irreversible transformation into cubic form during 1 day at 600 °C, but the transition was retarded at lower temperatures (Ivanov and Sapozhnikov 1985). Therefore, the formation of slyudyankaite might occur under recrystallization of primary cubic lazurite. Relatively low temperature and elevated SO_2 fugacity facilitated oxidation of sulfide sulfur (S_x^-) to S^0 species (S_6 and S_4), ordering of extra-framework species and related symmetry lowering.

It should be noted that slyudyankaite and vladimirivanovite are characterized by a number of common genetic and morphological features, indicating close conditions of their formation, other than for cubic lazurite. The latter usually dominates in classical bimetasomatic lazurite-bearing assemblages developed in contacts of dolomite marbles with granites (Korzhinsky, 1947). Slyudyankaite and vladimirivanovite are confined to recrystallization zones of early apocalciphyre lazurite metasomatites. Based on the relationships in thin sections, one can conclude that slyudyankaite is a later and, accordingly, low-temperature mineral relative to lazurite.

It is to be noted that a high content of HS^- anions in sodalite-group minerals is an indicator of highly reducing conditions of its formation (Chukanov et al., 2022). This anion which can be easily detected by Raman spectroscopy, occurs in slyudyankaite in trace amounts. This fact and the presence of extra-framework CO_2 molecules along with polysulfide species indicate that slyudyankaite crystallized under moderately reducing conditions.

Comparative data for slyudyankaite and other S-bearing aluminosilicate minerals structurally related to sodalite are given in Table 14.

IMPLICATIONS

The data obtained in this work using a multi-methodic approach made it possible to extend knowledge on the chemistry of sulfur in sodalite-group minerals. In slyudyankaite, sulfide sulfur occurs as the cyclic neutral species S_6 (the major form), subordinate *cis*- and *trans*-

conformers of the S_4 molecule as well as trace amounts of the $S_2^{\bullet-}$, $S_3^{\bullet-}$ and $S_4^{\bullet-}$ radical anions. Slyudyankaite is the first sodalite-group mineral in which S_6 and CO_2 molecules are the species-defining components. The occurrence of the large S_6 molecule in the structure results in the ordering of sulfide and sulfate sulfur and symmetry lowering to triclinic one. The color of different slyudyankaite varieties is determined by different combinations of chromophores, S_6 (pale yellow), $S_2^{\bullet-}$ (yellow), $S_3^{\bullet-}$ (deep blue), $S_4^{\bullet-}$ (red), and S_4 (red). Polychromism is also inherent to the orthorhombic lazurite-related mineral vladimirivanovite. The variations in coloration may be also due to the moderate redox conditions of mineral formation which are suitable for the simultaneous formation of different polysulfide chromophores. Some faint-colored lazurite varieties can get a more intense coloration as a result of the treatment under corresponding redox conditions and temperatures.

Another implication concerns evaluation of redox conditions of the metasomatic processes. The ratio of sulfide and sulfate sulfur may depend on oxygen and sulfur dioxide fugacities during lazurite formation (Lo Giudice et al. 2017, Sapozhnikov et al. 2021a). So-called "clathrasil" minerals like scapolite, sodalite, hackmanite, lazurite and other with closed cages hosted by clusters and molecules in aluminosilicate frameworks are appropriate to extract information about physicochemical conditions of mineral formation processes. However, the lack of reliable experimental calibration of the dependence between the fugacity *f* of a volatile component and composition of extra-framework components substantially confines such application. In the case of sodalite-group minerals from lazurite deposits, an experimental calibration was obtained using XPS referring to the redox index defined as the ratio of the integrated intensities of the XPS bands corresponding to sulfide groups (forms S^{2-}, $S_2^{\bullet-}$, $S_3^{\bullet-}$, S_4, etc.) and O-bearing groups (SO_3^{2-}, SO_4^{2-}, $S_2O_3^{2-}$) (Tauson et al. 2011). In the case of slyudyankaite, the redox index is equal to 0.1 (from the XPS data, Fig. 8) which corresponds to the fSO_2 and fO_2 values at 550 °C of ~10^{-3} and ~10^{-19} bar, respectively (Tauson et al. 2011). These values support the formation of slyudyankaite at moderately reducing conditions.

ACKNOWLEDGMENTS

The crystal structure investigation (by N.B.B.), ESR, NIR – Vis – US absorption and photo luminescence study (by R.Yu.S.) as well as Raman spectroscopy (by M.F.V. and N.V.C.) and analytical data processing (by N.V.C.) were supported by the Russian Science Foundation, grant No. 22-17-00006. The XPS study was performed within the framework of state-ordered project No. 0284-2021-0002. The IR spectroscopy study and analyses of H_2O and CO_2 were carried out by N.V.C. in accordance with the state task, state registration No. AAAA-A19-119092390076-7. The facilities of Shared Research Center 'Isotope-geochemical researches' in Vinogradov Institute of Geochemistry were extensively used. The authors would like to thank Prof. Wulf Depmeier and anonymous reviewer for their deep insight into the problem, constructive criticism and useful comments.

REFERENCES CITED

Billmers, R.I. and Smith, A.L. (1991) Ultraviolet-visible absorption spectra of equilibrium sulfur vapor: molar absorptivity spectra of S_3 and S_4. *The Journal of Physical Chemistry,* 95(11), 4242–4245. DOI: 10.1021/j100164a015.

Bragin, J., Diem, M., Guthals, D., and Chang, S. (1977) The vibrational spectrum and lattice dynamics of polycrystalline ammonium hydrosulfide. *Journal of Chemical Physics*, 67, 1247–1256. https://doi.org/10.1063/1.434936

Bruker APEX2, version 2.0-2; Bruker AXS Inc., Madison, Wisconsin, 2007a.

Bruker SAINT, version 6.0; Bruker AXS Inc., Madison, Wisconsin, 2007b.

Bokiy, G.B. and Borutskiy, B.E. (eds.) (2003) *Minerals*. Vol. V(2): *Framework Silicates*. Moscow, Nauka, 379 pp. (in Russian).

Bonaccorsi, E. and Merlino, S. (2005) Modular microporous minerals: Cancrinite-davyne group and C-S-H phases. *Reviews in Mineralogy and Geochemistry*, 57, 241–290.

Burragato, F., Maras, A., and Rossi, A. (1982) The sodalite group minerals in the volcanic areas of Latium. *Neues Jahrbuch für Mineralogie, Monatshefte*, 433–445.

Chukanov, N.V., Vigasina, M.F., Zubkova, N.V., Pekov, I.V., Schäfer, C., Kasatkin, A.V., Yapaskurt, V.O., and Pushcharovsky, D.Yu. (2020a) Extra-framework content in sodalite-group minerals: Complexity and new aspects of its study using infrared and Raman spectroscopy. *Minerals*, 10, 363. https://doi.org/10.3390/min10040363.

Chukanov, N.V., Sapozhnikov, A.N., Shendrik, R.Yu., Vigasina, M.F., and Steudel, R. (2020b) Spectroscopic and crystal-chemical features of sodalite-group minerals from gem lazurite deposits. *Minerals*, 10, 1042. https://doi.org/10.3390/min10111042.

Chukanov, N.V., Zubkova, N.V., Pekov, I.V., Shendrik, R.Yu., Varlamov, D.A., Vigasina, M.F., Belakovskiy, D.I., Britvin, S.N., Yapaskurt, V.O., Pushcharovsky, D.Yu. (2022a) Sapozhnikovite, $Na_8(Al_6Si_6O_{24})(HS)_2$, a new sodalite-group mineral from the Lovozero

alkaline massif, Kola Peninsula. *Mineralogical Magazine*, https://doi.org/10.1180/mgm.2021.94

Chukanov, N.V., Vigasina, M.F., Shendrik, R.Yu., Varlamov, D.A., Pekov, I.V., Zubkova, N.V. Nature and isomorphism of extra-framework components in cancrinite- and sodalite-related minerals: new data. *Minerals*, 2022b, 12, paper 729. https://doi.org/10.3390/min12060729

Clark, R.J.H., Dines, T.J., and Kurmoo, M. (1983) On the nature of the sulfur chromophores in ultramarine blue, green, violet, and pink and of the selenium chromophore in ultramarine selenium: Characterization of radical anions by electronic and resonance Raman spectroscopy and the determination of their excited-state geometries. *Inorganic Chemistry*, 22, 2766–2772.

Deer, W.A., Howie, R.A., and Zussman, J. (1963) *Rock-forming Minerals*. Vol. 4: *Framework Silicates*, 289–302.

Dubois, P., Lelieur, J. P., and Lepoutre, G. (1989) The solubilization process of sulfur in liquid ammonia and the equilibrium state of these solutions. *Inorganic Chemistry,* 28(2), 195–200. DOI:10.1021/ic00301a008.

Eckert, B. and Steudel, F. (2003) Molecular spectra of sulfur molecules and solid sulfur allotropes. *Topics in Current Chemistry,* 231, 31–97. DOI: 10.1007/b13181.

Evsyunin, V.G., Sapozhnikov, A.N., Kashaev, A.A., Rastsvetaeva, R.K. (1997) Crystal structure of triclinic lazurite. *Crystallography Reports*, 42, 938–945. https://dx.doi.org/10.1134/1.170716

Evsyunin, V.G., Rastsvetaeva, R.K., Sapozhnikov, A.N., Kashaev, A.A. (1998) Modulated structure of orthorhombic lazurite. *Crystallography Reports*, 43, 999–1002. http://dx.doi.org/10.1134/1.170884

Hassan, I. and Grundy, H.D. (1989) The structure of nosean, ideally $Na_8[Al_6Si_6O_{24}]SO_4 \cdot H_2O$. *The Canadian Mineralogist*, 27, 165–172.

Hogarth, D.D. and Griffin, W.L. (1976) New data on lazurite. *Lithos*, 9, 39–54.

Ivanov, V.G. and Sapozhnikov, A.N. (1985) *Lazurites of the USSR*. Nauka, Novosibirsk, 172 pp. (in Russian).

Jug, K. and Iffert, R. (1989) SINDOl study of sulphur isomers and sulphur fluorine compounds. *Journal of Molecular Structure (TheoChem),* 186*,* 347−359.

Kaneva, E.V., Cherepanov, D.I., Suvorova, L.F., Sapozhnikov, A.N., Levitskii, V.I. (2010) Orthorhombic lazurite from the Tultuiskoe deposit, Baikal Laake area. *Zapiski Rossiiskogo Mineralogicheskogo Obshchestva* (*Proceedings of the Russian Mineralogical Society*), 139(4), 95–101 (in Russian).

Kirk, R.D., Schulman, J.H., and Rosenstock, H.B. (1965) Structure in the luminescence emission of the S_2^- ion. *Solid State Communications*, 3(9), 235–239.

Korzhinsky, D.S. (1947) Archean bimetasomatic phlogopite and lazurite deposits of the Baikal Lake area. *Proceedings of the Institute of Geosciences, Academy of Sciences of the USSR, Petrographic Series*, 29(10), 1–163.

Kuribayashi, T., Aoki, S., and Nagase, T. (2018) Thermal behavior of modulated haüyne from Eifel, Germany: *In situ* high-temperature single-crystal X-ray diffraction study. *Journal of Mineralogical and Petrological Sciences*, 113, 51–55.

Levillain, E., Leghie, P., Gobeltz, N., and Lelieur, J.P. (1997) Identification of the $S_4^{\bullet-}$ radical anion in solution. *New Journal of Chemistry*, 21, 335−341.

Ling, Z.C., Wang, A., and Jolliff, B.L. (2011) Mineralogy and geochemistry of four lunar soils by laser-Raman study. *Icarus*, 211(1), 101–113.

Lo Giudice A, Angelici D, Re A, Gariani G, Borghi A, Calusi S, Giuntini L, Massi M, Castelli L, Taccetti F, Calligaro T, Pacheco C, Lemasson Q, Pichon L, Moignard B, Pratesi G, Guidotti MC (2017) Protocol for lapis lazuli provenance determination: evidence for an Afghan origin of the stones used for ancient carved artefacts kept at the Egyptian

Museum of Florence (Italy). *Archaeological and Anthropological Science*, 9, 637–651. https://doi.org/10.1007/s12520-016-0430-0

Löhn, J. and Schulz, H. (1968) Strukturverfeinerung am gestörten Haüyn, $(Na_5K_1Ca_2)Al_6Si_6O_{24}(SO_4)_{1.5}$. *Neues Jahrbuch für Mineralogie, Abhandlungen*, 109, 201–210 (in German with English abstract).

Momma, K. and Izumi, F. (2011) VESTA 3 for three-dimensional visualization of crystal, volumetric and morphology data. *Journal of Applied Crystallography*, 44, 1272–1276.

Norrbo, I., Gluchowski, P., Paturi, P., Sinkkonen, J., and Lastusaari, M. (2015) Persistent luminescence of tenebrescent $Na_8Al_6Si_6O_{24}(Cl,S)_2$: Multifunctional optical markers. *Inorganic Chemistry*, 54(16), 7717–7724. DOI: 10.1021/acs.inorgchem.5b00568.

Norrbo, I., Gluchowski, P., Hyppänen, I., Laihinen, T., Laukkanen, P., Mäkelä, J., Mamedov, G., Santos, H.S., Sinkkonen, J., Tuomisto, M., Viinikanoja, A., and Lastusaari, M. (2016) Mechanisms of tenebrescence and persistent luminescence in synthetic hackmanite $Na_8Al_6Si_6O_{24}(Cl,S)_2$. *ACS Applied Materials & Interfaces*, 8, 11592−11602. https://doi.org/10.1021/acsami.6b01959.

Paniz, H. and Lester, A. (1992) Vibronic absorption spectra of S_3 and S_4, in solid argon. *Journal of Physical Chemistry*, 96, 6579−6585.

Rejmak, P. (2020) Computational refinement of the puzzling red tetrasulfur chromophore in ultramarine pigments. *Physical Chemistry, Chemical Physics*. DOI: 10.1039/D0CP03019H.

Sapozhnikov, A.N. (1990) Indexing of additional reflections on the X-ray Debye diffraction patterns of lazurite concerning the study of modulation of its structure. *Zapiski Vsesoyuznogo Mineralogicheskogo Obshchestva* (*Proceedings of the Soviet Mineralogical Society*), 119(1), 110–116 (in Russian).

Sapozhnikov, A.N. (1992) Modulated structure of lazurite from deposits in southwestern Pamir. *Soviet Physical Crystallography*, 37, 470–472.

Sapozhnikov, A.N., Kaneva, E.V., Cherepanov, D.I., Suvorova, L.F., Ivanova, L.A., and Reznitsky, L.Z. (2012) Vladimirivanovite $Na_6Ca_2[Al_6Si_6O_{24}]$ $(SO_4,S^{-3},S^{-2},Cl)_2 \cdot H_2O$, a new mineral of sodalite group. *Geology of Ore Deposits*, 54, 557–564. https://doi.org/10.1134/S1075701512070070.

Sapozhnikov, A.N., Tauson, V.L., Lipko, S.V., Shendrik, R.Yu., Levitskii, V.I., Suvorova, L.F., Chukanov, N.V., and Vigasina, M.F. (2021a) On the crystal chemistry of sulfur-rich lazurite, ideally $Na_7Ca(Al_6Si_6O_{24})(SO_4)(S_3)^{-} \cdot nH_2O$. *American Mineralogist*, 106, 226–234. DOI: 10.2138/am-2020-7317.

Sapozhnikov, A.N., Chukanov, N.V., Shendrik, R.Yu., Vigasina, M.F., Tauson, V.L., Lipko, S.V., Belakovskiy, D.I., Levitskii, V.I., Suvorova, L.F., and Ivanova, L.A. (2021b) Lazurite: confirmation of the status of a mineral species with the formula $Na_7Ca(Al_6Si_6O_{24})(SO_4)$ $S_3^{\bullet -} \cdot H_2O$ and new data. *Zapiski Rossiiskogo Mineralogicheskogo Obshchestva* (*Proceedings of the Russian Mineralogical Society*), 150(4), 92–102 (in Russian). DOI: 10.31857/S0869605521040055.

Sheldrick, G.M. (2003) *SADABS, Program for empirical absorption correction of area detector data*. University of Göttingen, Germany.

Sheldrick, G.M. (2008) *XPREP, version 2008/2. Bruker-AXS*. Madison, Wisconsin, USA.

Sheppard, N. (1949) The assignment of the vibrational spectra of ethyl mercaptan and the ethyl halides, and the characterization of an SH deformation frequency. *The Journal of Chemical Physics*, 17, 79–83. DOI: 10.1063/1.1747057.

Steidel, J., Pickardt, J., and Steudel, R. (1978) Redetermination of the crystal and molecular structure of cyclohexasulfur, S_6. *Zeitschrift für Naturforschung*, Part B, 33, 1554–1555.

Steudel, R., Jensen, D., Göbel, P., and Hugo, P. (1988) Optical absorption spectra of the homocyclic sulfur molecules S_n (n = 6, 7, 8, 9, 10, 12, 15, 20) in solution. *Berichte der Bunsengesellschaft für physikalische Chemie*, 92, 118–122. https://doi.org/10.1002/bbpc.198800031.

Steudel, R. (2003) Inorganic polysulfides S_n^{2-} and radical anions $S_n^{\bullet-}$. In: Steudel R (ed.) Elemental Sulfur und Sulfur-Rich Compounds II. Topics in Current Chemistry, vol 231. Springer, Berlin – Heidelberg.

Steudel, R. and Chivers, T. (2019) The role of polysulfide dianions and radical anions in the chemical, physical and biological sciences, including sulfur-based batteries. *Chemical Society Reviews*, 48, 3279–3319 and 4338.

Tauson, V.L., Akimov, V.V., Sapozhnikov, A.N., and Kuznetsov, K.E. (1998) Investigation of the stability conditions and structural-chemical transformations of Baikal lazurite. *Geochemistry International*, 36, 717–733.

Tauson, V.L., Sapozhnikov, A.N., Shinkareva, S.N., and Lustenberg, E.E. (2011) Indicative properties of lazurite as a member of clathrasil mineral family. *Doklady Earth Sciences*, 441, 1732-1737. DOI: 10.1134/S1028334X11120312.

Tauson, V.L., Goettlicher, J., Sapozhnikov, A.N., Mangold, S., and Lustenberg, E.E. (2012) Sulfur speciation in lazurite-type minerals $(Na,Ca)_8[Al_6Si_6O_{24}](SO_4,S)_2$ and their annealing products: A comparative XPS and XAS study. *European Journal of Mineralogy*, 24, 133–152. https://doi.org/10.1127/0935-1221/2011/0023-2132

Tauson, V.L., Sapozhnikov, A.N., Kaneva, E.V., and Lipko, S.V. (2014) Reversion of incommensurate modulation in cubic lazurite: Example of reversible forced equilibrium? *Natural Resources*, 5, 761-771. http://dx.doi.org/10.4236/nr.2014.512065.

Taylor, D. (1967) The sodalite group of minerals. *Contributions to Mineralogy and Petrology*, 16, 172–188.

Tossel, J.A. (2003) Calculation of the visible-UV absorption spectra of hydrogen sulfide, bisulfide, polysulfide and As and Sb sulfides in aqueous solution. *Geochemistry Transaction*, 4(5), 28–33. DOI: 10.1039/b305086f.

Tubergen, M.J., Lavrich, R.J., and McCargar, J.W. (2000) Infrared spectrum and group theoretical analysis of the vibrational modes of carbonyl sulfide. *Journal of Chemical Education*, 2000, 77, 1637–1639.

Voskoboinikova, N.V. (1938) On the mineralogy of the Slyudyanskoe lazurite deposit. *Zapiski Rossiiskogo Mineralogicheskogo Obshchestva* (*Proceedings of the Russian Mineralogical Society*), 67(4), 601–622 (in Russian).

Weser, G., Hensel, F., and Warren, W.W. (1978) The optical absorption spectrum of fluid sulfur up to supercritical conditions. *Berichte der Bunsengesellschaft für physikalische Chemie*, 82(6), 588–594. DOI: 10.1002/bbpc.197800123.

Wong, M.W. and Steudel, R. (2003) Structure and spectra of tetrasulfur S_4 – an *ab initio* MO study. *Chemical Physics Letters*, 379, 162–169. DOI:10.1016/j.cplett.2003.08.026.

Wujcik, K.H., Wang, D.R., Raghunathan, A., Drake, M., Pascal, T.A., Prendergast, D., and Nitash Balsara, P. (2016) *Journal of Physical Chemistry C*, 120(33), 18403–18410. https://doi.org/10.1021/acs.jpcc.6b04264.

This is the peer-reviewed, final accepted version for American Mineralogist, published by the Mineralogical Society of America.
The published version is subject to change. Cite as Authors (Year) Title. American Mineralogist, in press.
DOI: https://doi.org/10.2138/am-2022-8598. http://www.minsocam.org/

FIGURE CAPTIONS

FIGURE 1. Slyudyankaite: (a) grains (bluish green to pale blue) in metasomatic rock with lazurite (dark blue), calcite (white), and pyrite (yellow), and (b) a fragment of holotype. The FOV widths are (a) 1.5 cm and (b) 0.8 mm.

FIGURE 2. Powder infrared absorption spectra of (*a*) slyudyankaite, (*b*) haüyne $(Na_{5.52}K_{0.35}Ca_{1.99})(Si_{6.10}Al_{5.81}Fe^{3+}_{0.09}O_{24})(SO_4)_{1.97}Cl_{0.11}\cdot nH_2O$ (Chukanov et al. 2020b) from the Laach Lake volcano, Eifel paleovolcanic region, Germany, and (*c*) lazurite neotype sample $(Na_{6.97}Ca_{0.88}K_{0.10})(Al_{5.96}Si_{6.04}O_{24})(SO_4^{2-})_{1.09}(S_3^{\bullet-})_{0.55}S^{2-}_{0.05}Cl_{0.04}\cdot 0.72H_2O$ from the Malo-Bystrinskoe deposit, Baikal Lake area. In the inset, IR spectrum of slyudyankaite in the range of 1500 – 3800 cm^{-1} is shown. The spectra are offset for comparison.

FIGURE 3. Raman spectrum of the slyudyankaite holotype sample.

FIGURE 4. ESR spectrum (first derivative) of the slyudyankaite holotype sample.The inset shows the dependence of the $S_3^{\bullet-}$ content in sodalite-group minerals (after Chukanov et al. 2020b – triangles) on measured doubly integrated ESR signal intensity obtained under similar conditions. The circle corresponds to slyudyankaite.

FIGURE 5. UV–Vis–near IR absorption spectra of (*a*) slyudyankaite holotype (greenish-blue) sample and (*b*) green slyudyankaite variety.

FIGURE 6. Fragment of a peripheral part of a green slyudyankaite grain. FOV width 150 μm.

FIGURE 7. Emission spectrum of green slyudyankaite under 405 nm excitation at 77 K.

FIGURE 8. The S2p XPS spectum of slyudyankaite.

FIGURE 9. Comparison of the shapes of the diffraction peaks of slyudyankaite (black) and cubic lazurite with a = 9.071 Å (red). Lazurite peaks are marked with the indices $(hkl)_{cub}$. The interplanar distances d for the slyudyankaite peaks are indicated on the bottom (see Table 4).

FIGURE 10. The crystal structure of slyudyankaite (general view in *ac* and *bc* projections). The unit cell is outlined. AlO_4 tetrahedra are blue-green, SiO_4 tetrahedra are orange, and SO_4

tetrahedra are yellow. The symbols 1 and 2 denote sodalite cages that do not contain SO_4^{2-} anions.

FIGURE 11. Three nonequivalent S_6 molecules in sodalite cages (*bc* projection). The symbols 1 and 2 denote sodalite cages. Cages # 1 contains S_6 molecules in two orientations (a, b), while S_6 molecules in Cages # 2 are equally oriented (c).

FIGURE 12. Three nonequivalent S_6 molecules in the sodalite cages # 1 and # 2 (*ac* projection).

FIGURE 13. Scheme of hypothetical mutual arrangement of H_2O and CO_2 molecules involved in strong dipole-dipole interactions.

TABLE 1. Data on the single-crystal XRD experiment and structure refinement details.

Crystal data	
Chemical formula	$Na_{28}Ca_4(Si_{24}Al_{24}O_{96})(SO_4)_6S_{2.04+x}(H_2O)_y(CO_2)_z$ *
M_r	4303.6
Crystal system, space group	Triclinic, *P*1
Temperature (K)	170
a, *b*, *c* (Å)	9.0523(4), 12.8806(6), 25.681(1)
α, β, γ (degrees)	89.988(2), 90.052(1), 90.221(1)
V (Å^3)	2994.4(2)
Z	1
Radiation type	X-ray, λ = 0.7107 Å
μ (mm^{-1})	0.986
Crystal shape	prismatic
Crystal size (mm)	0.200× 0.165× 0.143
Data collection	
Diffractometer	Bruker AXS D8 VENTURE
Absorption correction	multi-scan
T_{min}, T_{max}	0.9295, 1.000
No. of reflections measured	75692
$(\sin\theta/\lambda)_{max}$ (Å^{-1})	0.911
Refinement details	
Refinement technique	LSQ based on *F*
Weighting sceme	$w = 1/[\sigma^2(F_{obs}) + (0.05F_{obs})^2]$
No. of all reflections	37942
No. of observed [$I > 3\sigma(I)$] reflections	35297
R (all, obs)**, %	4.64, 4.28
wR (all, obs)**, %	7.58, 7.38

This is the peer-reviewed, final accepted version for American Mineralogist, published by the Mineralogical Society of America.
The published version is subject to change. Cite as Authors (Year) Title. American Mineralogist, in press.
DOI: https://doi.org/10.2138/am-2022-8598. http://www.minsocam.org/

GOF (all, obs)**	1.32, 1.34
No. of parameters	1926
No. of restraints	0
No. of constraints	106
$\Delta\rho_{max}$, $\Delta\rho_{min}$ (e Å^{-3})	2.38, -1.69

* The parameters *x*, *y*, and *z* are related to residual electron density (not refined)

** $R(F) = \frac{\sum ||F|_{obs} - |F|_{calc}|}{\sum |F|_{obs}}$; $wR(F) = \sqrt{\frac{\sum [w(|F|_{obs} - |F|_{calc})]^2}{\sum (w|F|_{obs}^{\ 2})}}$; $GOF = \sqrt{\frac{\sum [w(|F|_{obs} - |F|_{calc})^2]}{N-P}}$

This is the peer-reviewed, final accepted version for American Mineralogist, published by the Mineralogical Society of America.
The published version is subject to change. Cite as Authors (Year) Title. American Mineralogist, in press.
DOI: https://doi.org/10.2138/am-2022-8598. http://www.minsocam.org/

TABLE 2. Raman bands of slyudyankaite and their assignment.

Raman shift (cm^{-1})	Assignment
219	*trans*-S_4 bending
255	$S_3^{\bullet-}$ bending A_2 (ν_2) mode; S_6 molecule of D_{3d} symmetry, bending
284	Framework bending vibrations (resonance with a S_6 bending mode?)
298	Framework bending vibrations (overlapping with $S_4^{\bullet-}$ bending band?)
300	*cis*-S_4 mixed ν_4 mode (symmetric bending + stretching)
380 w	*cis*-S_4 mixed ν_3 mode
437	Broad band. Possibly, overlapping SO_4 [bending E (ν_2) mode] and S_6 (mixed mode) bands.
477	S_6 stretching mode (+ mixed ν_4 mode of *trans*-S_4 and framework bending vibrations)
503	Bending vibrations of four-membered aluminosilicate rings belonging to the framework (Ling et al. 2011).
545 s	$S_3^{\bullet-}$ symmetric stretching (ν_1) (possibly, overlapping with the stretching band of *gauche*-S_4)
580	$S_3^{\bullet-}$ antisymmetric stretching (ν_3)
614	SO_4 [bending F_2 (ν_4) mode]
645	*cis*-S_4 stretching
682	*trans*-S_4 symmetric stretching ν_3 mode
807	$S_3^{\bullet-}$ combination mode ($\nu_1 + \nu_2$)
985 s	SO_4 [symmetric stretching A_1 (ν_1) mode])possibly, overlapping with the weak band of framework stretching vibrations)
1088 s	Asymmetric band. $S_3^{\bullet-}$ overtone ($2\times\nu_1$) [possibly, overlapping with weak $SO_4^{\bullet-}$ stretching bands ($\nu_3 - F_2$)]
1279 and 1381	Symmetric C–O stretching vibrations of CO_2 molecules (Fermi doublet, resonance with the overtone of CO_2 bending vibrations).
1340	Symmetric C–O stretching vibrations of CO_2 molecules – involved in strong dipole-dipole interactions (a single band because of the shift of the CO_2 bending band due to the dipole-dipole interactions).
1631	$S_3^{\bullet-}$ overtone ($3\times\nu_1$)
1891	$S_3^{\bullet-}$ combination mode ($3\times\nu_1 + \nu_2$)
2172	$S_3^{\bullet-}$ overtone ($4\times\nu_1$)
2428 w	$S_3^{\bullet-}$ combination mode ($4\times\nu_2 + \nu_1$)
2575 w	Narrow band. H–S stretching vibrations.
2710	$S_3^{\bullet-}$ overtone ($5\times\nu_1$)
2964 w	$S_3^{\bullet-}$ combination mode ($5\times\nu_1 + \nu_2$)

3247 w	$S_3^{\bullet-}$ overtone ($6\times\nu_1$)

Note: w – weak band, s – strong band.

TABLE 3. Chemical composition of slyudyankaite

Constituent	Wt%	Range	Standard deviation
Na_2O	19.28	18.03 – 19.80	0.61
K_2O	0.12	0 – 0.23	0.07
CaO	5.13	4.96 – 5.52	0.19
Al_2O_3	27.01	26.70 – 27.75	0.38
SiO_2	33.25	32.82 – 33.82	0.36
SO_3*	10.94	14.98 – 15.72***	0.28
S**	1.75		
Cl	0.10	0.08 – 0.14	0.02
CO_2	1.42		
H_2O	0.90		
–O≡Cl	–0.03		
Total	**99.87**		

Note: *Sulfate sulfur determined by wet chemical analysis.

**Sulfide sulfur determined as the difference between total sulfur and sulfur determined by wet chemical analysis.

***For total sulfur determined as SO_3.

This is the peer-reviewed, final accepted version for American Mineralogist, published by the Mineralogical Society of America.
The published version is subject to change. Cite as Authors (Year) Title. American Mineralogist, in press.
DOI: https://doi.org/10.2138/am-2022-8598. http://www.minsocam.org/

TABLE 4. Powder X-ray diffraction data of slyudyankaite (this work) and green "triclinic lazurite" (Ivanov and Sapozhnikov, 1985; ICDD card 041-1392).

Slyudyankaite (holotype)				"Triclinic lazurite"		*hkl*
I_{meas}, %	d_{meas}, Å*	I_{calc}, %**	d_{calc}, Å	I_{meas}, %	d_{meas}, Å	
6	12.93	20	12.88	10	12.8	010
4	11.49	3	11.51	5	11.6	011
3	9.10	12	9.05	8	9.08	100
3	7.43	7	7.42	8	7.44	110
2	7.12	2	7.10	4	7.14	111
11	6.45	20	6.43	40	6.43	020
2	5.62	1	5.61	2	5.66	113
3	4.869	3	4.861	2	4.861	114
5	4.551	3	4.547	15	4.55	200
3	4.223	3	4.229	10	4.225	115
3	4.069	3	4.067	8	4.069	212
2	4.014	2	4.017	5	4.013	203
100	3.716	100	3.713	100	3.714	204
2	3.405	4	3.407	8	3.401	205
2	3.296	3	3.293	7	3.295	117
2	3.211	1	3.215	-	-	040
4	3.122	4	3.119	10	3.120	206
3	3.032	3	3.031	9	3.029	232
12	2.878	11	2.876	40	2.876	312
2	2.674	1	2.667	2	2.670	137
23	2.625	28	2.625	80	2.624	208
2	2.521	1	2.522	2	2.522	236
6	2.431	3	2.430	20	2.429	152
6	2.275	5	2.274	15	2.273	400
3	2.235	2	2.230	6	2.230	410
12	2.143	11	2.143	40	2.143	420
2	2.110	2	2.114	3	2.107	414
2	2.086	1	2.086	1	2.085	149
-	-	2	2.05	4	2.052	157
-	-	2	2.00	3	2.003	1.3.11
2	1.961	1	1.961	1	1.961	158
2	1.937	2	1.939	4	1.937	260
1	1.916	1	1.912			353
2	1.872	1	1.876			354
2	1.853	1	1.851			427
2	1.838	-	1.833			31.11

1	1.820	1	1.814			265
7	1.784	9	1.783			512
2	1.660	4	1.660			532
5	1.607	9	1.608			080
3	1.559	-	1.560			084
2	1.517	2	1.516			600
3	1.475	-	1.475			552
5	1.3713	5	1.3710			288
2	1.3400	-	1.3408			644
3	1.3116	3	1.3126			440
2	1.2857	-	1.2861			712
3	1.2375	3	1.2375			732

* For the unit-cell parameters calculated from powder data.

** Total integrated values for groups of overlapping reflections.

This is the peer-reviewed, final accepted version for American Mineralogist, published by the Mineralogical Society of America.
The published version is subject to change. Cite as Authors (Year) Title. American Mineralogist, in press.
DOI: https://doi.org/10.2138/am-2022-8598. http://www.minsocam.org/

TABLE 5. The site occupancies, positional (*x/a, y/b, z/c*) and isotropic/equivalent atomic displacement parameters for the sulfate (S, Os) and sulfide (Ss) groups.

Atom	Occupancy	*x/a*	*y/b*	*z/c*	*U*(iso*/eq), Å^2
S1	1	0.98658(10)	0.00439(7)	0.61028(3)	0.01232(9)*
Os11	1	0.1337(3)	–0.0069(3)	0.58744(14)	0.0342(8)
Os12	1	0.8758(4)	0.0214(3)	0.56999(13)	0.0387(10)
Os13	1	0.9525(3)	0.9111(2)	0.64099(11)	0.0255(6)
Os14	1	0.9839(5)	0.0946(2)	0.64552(13)	0.0367(9)
S2	1	0.05780(10)	0.46740(7)	0.87680(3)	0.01223(9)*
Os21	1	0.0640(4)	0.5431(3)	0.92030(11)	0.0352(9)
Os22	1	0.0909(3)	0.5236(2)	0.82814(9)	0.0238(6)
Os23	1	0.1700(4)	0.3891(3)	0.88731(17)	0.0388(10)
Os24	1	–0.0917(3)	0.4222(3)	0.87353(12)	0.0296(7)
S3	1	0.52821(10)	0.03527(7)	0.88757(4)	0.01377(10)*
Os31	1	0.5246(5)	0.9588(3)	0.84609(13)	0.0398(10)
Os32	0.75	0.5702(5)	0.1416(3)	0.8707(2)	0.0371(13)
Os33	0.75	0.3767(5)	0.0501(4)	0.9107(2)	0.0425(14)
Os34	0.75	0.6332(5)	–0.0048(3)	0.92602(15)	0.0308(10)
Os35	0.25	0.6828(14)	0.0760(15)	0.8971(7)	0.053(5)
Os36	0.25	0.4850(18)	0.9906(12)	0.9407(5)	0.040(4)
Os37	0.25	0.4226(18)	0.1040(11)	0.8695(6)	0.042(4)
S4	1	0.95418(10)	0.53721(7)	0.37700(3)	0.01346(10)*
Os41	1	0.9593(4)	0.4563(3)	0.41870(12)	0.0360(9)
Os42	1	0.9160(3)	0.4839(2)	0.32813(10)	0.0251(6)
Os43	1	0.8405(4)	0.6121(3)	0.39126(17)	0.0390(10)
Os44	1	0.1016(3)	0.5856(3)	0.37258(14)	0.0367(9)
S5	1	0.01418(10)	1.00076(7)	1.11055(3)	0.01210(9)*
Os51	1	0.1311(4)	0.9824(3)	1.07270(15)	0.0425(11)
Os52	1	0.8707(3)	0.0176(3)	1.08505(13)	0.0300(7)
Os53	1	0.0478(4)	0.0924(2)	0.14235(12)	0.0278(7)
Os54	1	0.0059(5)	0.9108(2)	0.14602(15)	0.0413(11)
S6	1	0.47322(10)	–0.02916(7)	0.38684(4)	0.01520(10)*
Os61	1	0.4703(5)	0.0529(3)	0.34832(13)	0.0398(10)
Os62	0.5	0.4377(14)	0.8660(6)	0.3663(5)	0.067(4)
Os63	0.5	0.3516(12)	0.0066(8)	0.4214(3)	0.060(3)
Os64	0.5	0.6246(15)	–0.0415(10)	0.4098(6)	0.089(5)
Os65	0.5	0.5831(10)	0.8999(6)	0.3628(3)	0.046(2)
Os66	0.5	0.3362(9)	–0.0834(8)	0.3953(5)	0.063(3)
Os67	0.5	0.5394(12)	0.0081(7)	0.4367(3)	0.050(3)
Ss10	0.1219	0.4350(10)	0.3721(7)	0.6048(3)	0.0291(5)*
Ss11	0.1219	0.5206(10)	0.4053(7)	0.6784(3)	0.0291(5)*

Ss12	0.1219	0.6864(10)	0.5021(7)	0.6607(3)	0.0291(5)*
Ss13	0.1219	0.5695(10)	0.6301(7)	0.6384(3)	0.0291(5)*
Ss14	0.1219	0.4941(10)	0.5960(7)	0.5723(3)	0.0291(5)*
Ss15	0.1219	0.3257(10)	0.5021(7)	0.5887(3)	0.0291(5)*
Ss20	0.2188	0.6713(7)	0.4910(5)	0.0862(2)	0.0387(5)*
Ss21	0.2188	0.3195(7)	0.5092(5)	0.1611(2)	0.0387(5)*
Ss22	0.1094	0.4999(15)	0.5910(10)	0.0692(5)	0.0387(5)*
Ss23	0.1094	0.4189(15)	0.6358(10)	0.1401(5)	0.0387(5)*
Ss24	0.1094	0.5000(15)	0.4171(10)	0.1792(5)	0.0387(5)*
Ss25	0.1094	0.5677(15)	0.3745(10)	0.1089(5)	0.0387(5)*
Ss26	0.1094	0.5635(14)	0.6232(10)	0.0946(5)	0.0387(5)*
Ss27	0.1094	0.4807(15)	0.6080(9)	0.1732(5)	0.0387(5)*
Ss28	0.1094	0.4188(15)	0.3814(10)	0.1482(5)	0.0387(5)*
Ss29	0.1094	0.5220(15)	0.4020(10)	0.0756(5)	0.0387(5)*

This is the peer-reviewed, final accepted version for American Mineralogist, published by the Mineralogical Society of America.
The published version is subject to change. Cite as Authors (Year) Title. American Mineralogist, in press.
DOI: https://doi.org/10.2138/am-2022-8598. http://www.minsocam.org/

TABLE 6. The site occupancies, positional (*x/a, y/b, z/c*) and isotropic/equivalent atomic displacement parameters for the extra-framework cations.

Atom	Occupancy	x/a	y/b	z/c	u(eq), Å^2
Na1	1	–0.19173(15)	0.31830(10)	0.37490(5)	0.0145(3)
Na2	1	0.30447(16)	0.18251(11)	0.37469(5)	0.0157(3)
Na3	1	0.15573(15)	0.50919(10)	0.28072(5)	0.0161(3)
Na4	1	0.17786(16)	0.49512(11)	0.46802(7)	0.0216(3)
Na5	1	0.69832(16)	0.82803(11)	0.87228(5)	0.0163(3)
Na6	1	0.22866(18)	0.49604(11)	0.98725(7)	0.0242(4)
Na7	1	0.21754(17)	0.19037(12)	0.63225(5)	0.0195(3)
Na8	1	0.26832(16)	0.49197(10)	0.76090(6)	0.0187(3)
Na9	1	0.81192(16)	0.19132(11)	0.12885(5)	0.0164(3)
Na10	1	0.22443(18)	0.22212(14)	1.12320(5)	0.0228(4)
Na11	1	0.34750(16)	0.99768(10)	0.78291(6)	0.0179(3)
Na12	1	0.80643(19)	0.21886(16)	0.62196(6)	0.0300(4)
Na13	1	0.19925(14)	0.68712(10)	0.87470(5)	0.0130(2)
Na14	1	0.65346(17)	0.00616(11)	0.28424(6)	0.0189(3)
Na15	1	0.84822(15)	0.49767(10)	0.78213(5)	0.0152(3)
Na16	1	0.84816(15)	0.00407(10)	0.72185(5)	0.0142(3)
Na17	1	0.15986(16)	0.00334(10)	0.22198(5)	0.0161(3)
Na18	1	0.77836(18)	0.51319(10)	0.48455(7)	0.0220(3)
Na19	1	0.78046(17)	0.81087(13)	0.13135(6)	0.0213(3)
Na20	1	0.83342(16)	0.51095(11)	0.96678(6)	0.0188(3)
Na21	1	0.19632(16)	0.81805(11)	0.62904(6)	0.0187(3)
Na22	1	0.19394(18)	0.79241(14)	1.11886(6)	0.0249(4)
Na23	1	0.77838(17)	0.78003(13)	0.62168(5)	0.0208(3)
Na24	1	0.74221(17)	0.51136(10)	0.26041(6)	0.0196(3)
Ca25	0.75	0.32023(9)	0.24277(6)	0.87974(3)	0.01542(13)
Na25	0.25	0.32023(9)	0.24277(6)	0.87974(3)	0.01542(13)
Ca26	0.5	0.69924(12)	0.75691(8)	0.37732(3)	0.0227(2)
Na26	0.5	0.69924(12)	0.75691(8)	0.37732(3)	0.0227(2)
Ca27	0.75	0.76119(9)	0.00609(5)	1.00183(3)	0.01392(12)
Na27	0.25	0.76119(9)	0.00609(5)	1.00183(3)	0.01392(12)
Ca28	0.5	0.22524(10)	0.76011(7)	0.37589(3)	0.01693(17)
Na28	0.5	0.22524(10)	0.76011(7)	0.37589(3)	0.01693(17)
Ca29	0.5	0.72064(8)	0.00462(6)	0.49602(3)	0.01017(13)
Na29	0.5	0.72064(8)	0.00462(6)	0.49602(3)	0.01017(13)
Ca30	0.5	0.23748(13)	–0.00142(7)	0.50217(4)	0.0223(2)
Na30	0.5	0.23748(13)	–0.00142(7)	0.50217(4)	0.0223(2)
Na31	0.75	0.78328(13)	0.24868(9)	0.87676(4)	0.0181(2)
Ca31	0.25	0.78328(13)	0.24868(9)	0.87676(4)	0.0181(2)
Na32	0.75	0.28125(12)	0.00261(8)	0.99585(4)	0.0153(2)
Ca32	0.25	0.28125(12)	0.00261(8)	0.99585(4)	0.0153(2)

This is the peer-reviewed, final accepted version for American Mineralogist, published by the Mineralogical Society of America.
The published version is subject to change. Cite as Authors (Year) Title. American Mineralogist, in press.
DOI: https://doi.org/10.2138/am-2022-8598. http://www.minsocam.org/

TABLE 7. The S–S distances (Å), S–S–S angles, and S–S–S–S torsion angles (°) in the S_6 molecules.

Cage # 1, S_6 molecule in the first orientation		Cage # 1, S_6 molecule in the second orientation		Cage # 2	
S–S distances					
Ss20–Ss22	2.07(1)	Ss20–Ss26	1.98(1)	Ss10–Ss11	2.08(1)
Ss22–Ss23	2.05(2)	Ss26–Ss27	2.16(2)	Ss11–Ss12	2.00(1)
Ss23–Ss21	1.93(1)	Ss27–Ss21	1.96(1)	Ss12–Ss13	2.04(1)
Ss21–Ss24	2.07(1)	Ss21–Ss28	1.91(1)	Ss13–Ss14	1.88(1)
Ss24–Ss25	1.99(2)	Ss28–Ss29	2.10(2)	Ss14–Ss15	1.99(1)
Ss25–Ss20	1.86(1)	Ss29–Ss20	1.79(1)	Ss15–Ss10	1.99(1)
<S–S>	1.995	<S–S>	1.983	<S–S>	1.997
S–S–S angles					
Ss25–Ss20–Ss22	101.0(6)	Ss29–Ss20–Ss26	101.2(6)	Ss15–Ss10–Ss11	101.6(5)
Ss20–Ss22–Ss23	105.0(7)	Ss20–Ss26–Ss27	101.3(6)	Ss10–Ss11–Ss12	101.4(5)
Ss22–Ss23–Ss21	100.2(7)	Ss26–Ss27–Ss21	99.6(6)	Ss11–Ss12–Ss13	100.2(5)
Ss23–Ss21–Ss24	100.3(6)	Ss27–Ss21–Ss28	103.7(6)	Ss12–Ss13–Ss14	104.6(5)
Ss21–Ss24–Ss25	101.5(7)	Ss21–Ss28–Ss29	104.8(7)	Ss13–Ss14–Ss15	103.1(5)
Ss24–Ss25–Ss20	102.6(7)	Ss28–Ss29–Ss20	106.3(7)	Ss14–Ss15–Ss10	100.0(5)
<S–S–S>	101.8	<S–S–S>	102.8	<S–S–S>	101.8
Torsion S–S–S–S angles					
Ss20–Ss22–Ss23–Ss21	–72.8(7)	Ss20–Ss26–Ss27–Ss21	–75.6(7)	Ss10–Ss11–Ss12–Ss13	70.5(5)
Ss22–Ss23–Ss21–Ss24	73.3(7)	Ss26–Ss27–Ss21–Ss28	72.5(7)	Ss11–Ss12–Ss13–Ss14	–74.4(6)
Ss23–Ss21–Ss24–Ss25	–78.1(7)	Ss27–Ss21–Ss28–Ss29	–69.3(7)	Ss12–Ss13–Ss14–Ss15	77.2(6)
Ss21–Ss24–Ss25–Ss20	79.2(7)	Ss21–Ss28–Ss29–Ss20	71.5(8)	Ss13–Ss14–Ss15–Ss10	–77.3(6)
Ss24–Ss25–Ss20–Ss22	–74.5(7)	Ss28–Ss29–Ss20–Ss26	–73.7(7)	Ss14–Ss15–Ss10–Ss11	74.9(6)
Ss25–Ss20–Ss22–Ss23	72.7(7)	Ss29–Ss20–Ss26–Ss27	77.1(7)	Ss15–Ss10–Ss11–Ss12	–75.7(6)
<|S–S–S–S|>	75.1	<|S–S–S–S|>	73.3	<|S–S–S–S|>	75.0

This is the peer-reviewed, final accepted version for American Mineralogist, published by the Mineralogical Society of America.
The published version is subject to change. Cite as Authors (Year) Title. American Mineralogist, in press.
DOI: https://doi.org/10.2138/am-2022-8598. http://www.minsocam.org/

TABLE 8. Distances (Å) between S atoms of the S_6 rings and the nearest cation sites.

Cage # 1		Cage # 2, ring # 1		Cage # 2, ring # 2	
Ss10–Na7	3.13(1)	Ss20–Na20	3.41(1)	Ss20–Na20	3.41(1)
Ss1–Na8	3.31(1)	Ss22–Na6	3.45(1)	Ss26–Na19	3.25(1)
Ss12–Na18	3.44(1)	Ss23–Na22	2.92(1)	Ss27–Na24	3.49(1)
Ss13–Na23	2.73(1)	Ss21–Na3	3.41(1)	Ss21–Na3	3.41(1)
Ss14–Na18	3.59(1)	Ss24–Na24	3.26(1)	Ss28–Na10	2.77(1)
Ss15–Na4	3.37(1)	Ss25–Na9	3.28(1)	Ss29–Na6	3.70(1)

TABLE 9. Distances (Å) between S atoms of the S_6 rings and the nearest O atoms of the framework.

Cage # 1		Cage # 2, ring # 1		Cage # 2, ring # 2	
Ss10–O37	2.92(1)	Ss20–O87	3.14(1)	Ss20–O87	3.14(1)
Ss11–O62	3.10(1)	Ss22–O47	2.98(1)	Ss26–O67	3.08(1)
Ss12–O69	3.13(1)	Ss23–O86	2.96(1)	Ss27–O46	3.17(1)
Ss13–O65	2.84(1)	Ss21–O96	3.15(1)	Ss21–O96	3.15(1)
Ss14–O30	3.05(1)	Ss24–O25	2.81(1)	Ss28–O24	2.75(1)
Ss15–O54	3.09(1)	Ss25–O79	2.99(1)	Ss29–O27	3.13(1)

This is the peer-reviewed, final accepted version for American Mineralogist, published by the Mineralogical Society of America.
The published version is subject to change. Cite as Authors (Year) Title. American Mineralogist, in press.
DOI: https://doi.org/10.2138/am-2022-8598. http://www.minsocam.org/

TABLE 10. Comparative data for slyudyankaite and other S-bearing minerals with the $[Al_6Si_6O_{24}]$ framework having **SOD**-type topology.

Mineral	Slyudyankaite	Vladimirivanovite	Lazurite	Nosean	Haüyne	Sapozhnikovite
Formula	$Na_{28}Ca_4(Si_{24}Al_{24}O_{96})(SO_4)_6(S_6)_{1/3}(CO_2)\cdot 2H_2O$	$Na_6Ca_2(Al_6Si_6O_{24})(SO_4,S_3^{\bullet-},S_2^{\bullet-},Cl)\cdot H_2O$	$Na_7Ca(Al_6Si_6O_{24})(SO_4)S_3^{\bullet-}\cdot H_2O$*	$Na_8(Al_6Si_6O_{24})(SO_4)\cdot H_2O$	$Na_6Ca_2(Al_6Si_6O_{24})(SO_4)_2$	$Na_8(Al_6Si_6O_{24})(HS)_2$
Crystal system **Space group**	Triclinic *P*1	Orthorhombic *Pnaa*	Cubic $P\bar{4}3n$	Cubic $P\bar{4}3n$	Cubic $P\bar{4}3n$	Cubic $P\bar{4}3n$
Unit-cell parameters, Å/° ***V*, Å^3, *Z***	*a* = 9.0523, *b* = 12.8806, *c* = 25.681, α = 89.988, β = 90.052, γ = 90.221 *V* = 2994.4, 1	*a* = 9.066, *b* = 12.851, *c* = 38.558 4492, 6	*a* = 9.071 – 9.09 746.4 – 750.3, 1	*a* = 9.05 – 9.08 741 – 749.6, 1	*a* = 9.08 – 9.13 748.6 – 761.0, 1	*a* = 8.9146 708.45, 1
Strong lines in powder X-ray diffraction pattern: *d*, Å (*I*, %)	6.45 (11) 3.716 (100) 2.878 (12) 2.625 (23) 2.431 (6) 2.275 (6) 2.143 (12) 1.784 (7)	6.61 (5) 6.43 (11) 3.71 (100) 2.623 (30) 2.273 (6) 2.141 (14) 1.783 (9) 1.606 (6)	6.437 (18) 4.548 (8) 3.711 (100) 2.875 (16) 2.623 (30) 2.142 (16) 1.782 (9)	9.127 (10) 6.464 (36) 3.718 (100) 2.876 (24) 2.625 (49) 2.143 (25) 1.607 (11)	6.47 (16) 3.72 (100) 2.873 (14) 2.623 (25) 2.428 (8) 2.141 (14) 1.781 (10)	6.30 (37) 3.638 (100) 2.821 (14) 2.572 (18) 2.382 (16) 2.101 (29) 1.576 (8)
Optical data	Biaxial (+): α = 1.506, β = 1.509, γ = 1.513	Biaxial (+/–): α = 1.502 – 1.507, β = 1.509 – 1.514, γ = 1.512 – 1.517	Nearly isotropic: *n* = 1.502 – 1.522	Isotropic: *n* = 1.461 – 1.495	Isotropic: *n* = 1.494 – 1.509	Isotropic: *n* = 1.499
Density (g·cm^{-3})	2.46 (meas.) 2.454 (calc.)	2.48 (meas.) 2.436 (calc.)	2.38 – 2.45 (meas.) 2.39 – 2.42 (calc.)	2.25 – 2.40 (meas.)	2.44 – 2.50 (meas.).	2.25 (meas.) 2.247 (calc.)

This is the peer-reviewed, final accepted version for American Mineralogist, published by the Mineralogical Society of America.
The published version is subject to change. Cite as Authors (Year) Title. American Mineralogist, in press.
DOI: https://doi.org/10.2138/am-2022-8598. http://www.minsocam.org/

				2.21 (calc.)		
Sources	This work	Sapozhnikov et al. 2012	Deer et al. 1963, Hogarth and Griffin, 1976, Sapozhnikov 1990, Bokiy and Borutskiy 2003, Chukanov et al. 2020b, Sapozhnikov et al. 2021a,b	Deer et al. 1963, Taylor 1967, Hassan and Grundy 1989, Bokiy and Borutskiy 2003	Deer et al. 1963, Löhn and Schulz 1968, Burragato et al. 1982, Kuribayashi et al. 2018	Chukanov et al. 2022a

* The revised formula of lazurite was approved by the IMA CNMNC on March 2nd, 2021 (Nomenclature Voting proposal 20-H).

Note: The existence of analogues of slyudyankaite with different extra-framework anions and neutral molecules is possible. The probable variants are $Na_{28}Ca_4(Si_{24}Al_{24}O_{96})(SO_4)_6(S_4)_{1/2}(CO_2)\cdot 2H_2O$, $Na_{28}Ca_4(Si_{24}Al_{24}O_{96})(SO_4)_6(S_6)_{1/2}\cdot 2H_2O$, $Na_{28}Ca_4(Si_{24}Al_{24}O_{96})(SO_4)_6(CO_2)_3\cdot 2H_2O$, and $Na_{28}Ca_4(Si_{24}Al_{24}O_{96})(SO_4)_6\cdot nH_2O$.

This is the peer-reviewed, final accepted version for American Mineralogist, published by the Mineralogical Society of America.
The published version is subject to change. Cite as Authors (Year) Title. American Mineralogist, in press.
DOI: https://doi.org/10.2138/am-2022-8598. http://www.minsocam.org/

FIGURES

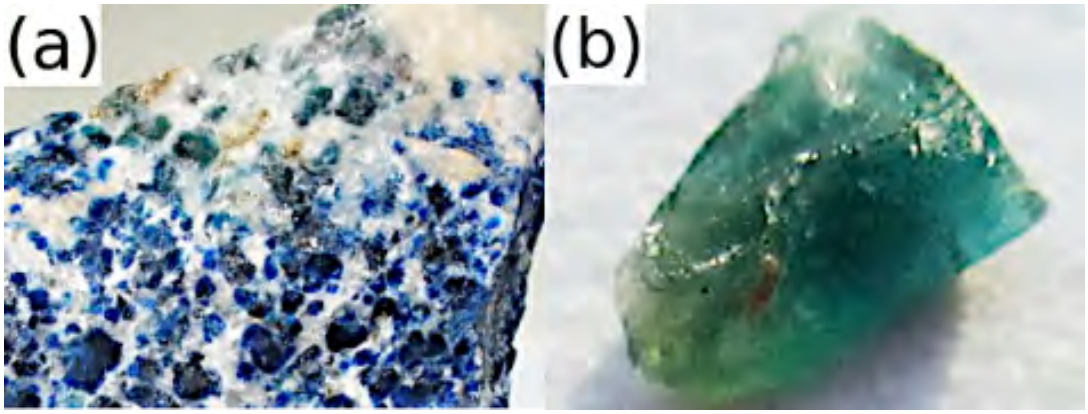

Figure 1

This is the peer-reviewed, final accepted version for American Mineralogist, published by the Mineralogical Society of America.
The published version is subject to change. Cite as Authors (Year) Title. American Mineralogist, in press.
DOI: https://doi.org/10.2138/am-2022-8598. http://www.minsocam.org/

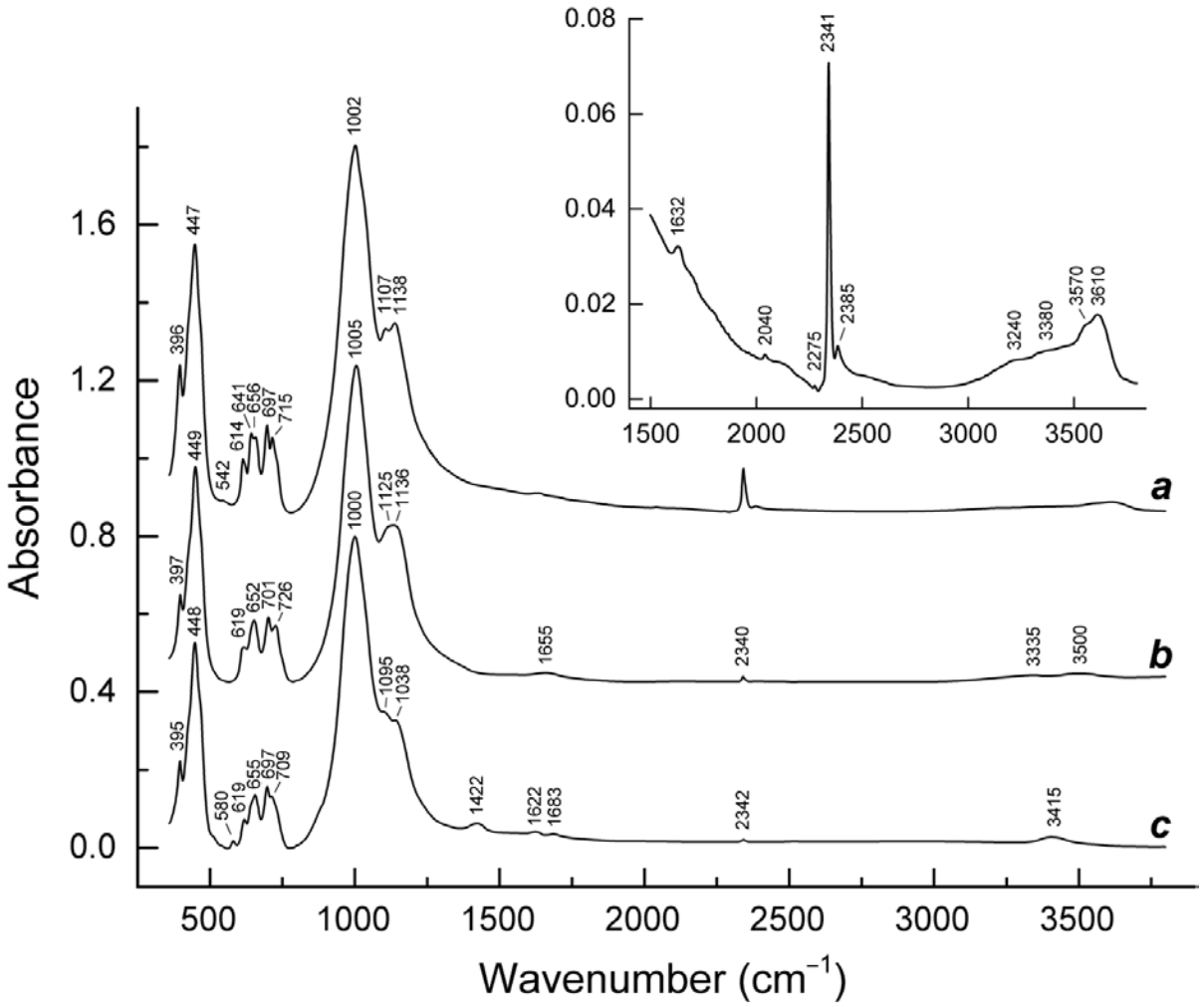

Figure 2

This is the peer-reviewed, final accepted version for American Mineralogist, published by the Mineralogical Society of America.
The published version is subject to change. Cite as Authors (Year) Title. American Mineralogist, in press.
DOI: https://doi.org/10.2138/am-2022-8598. http://www.minsocam.org/

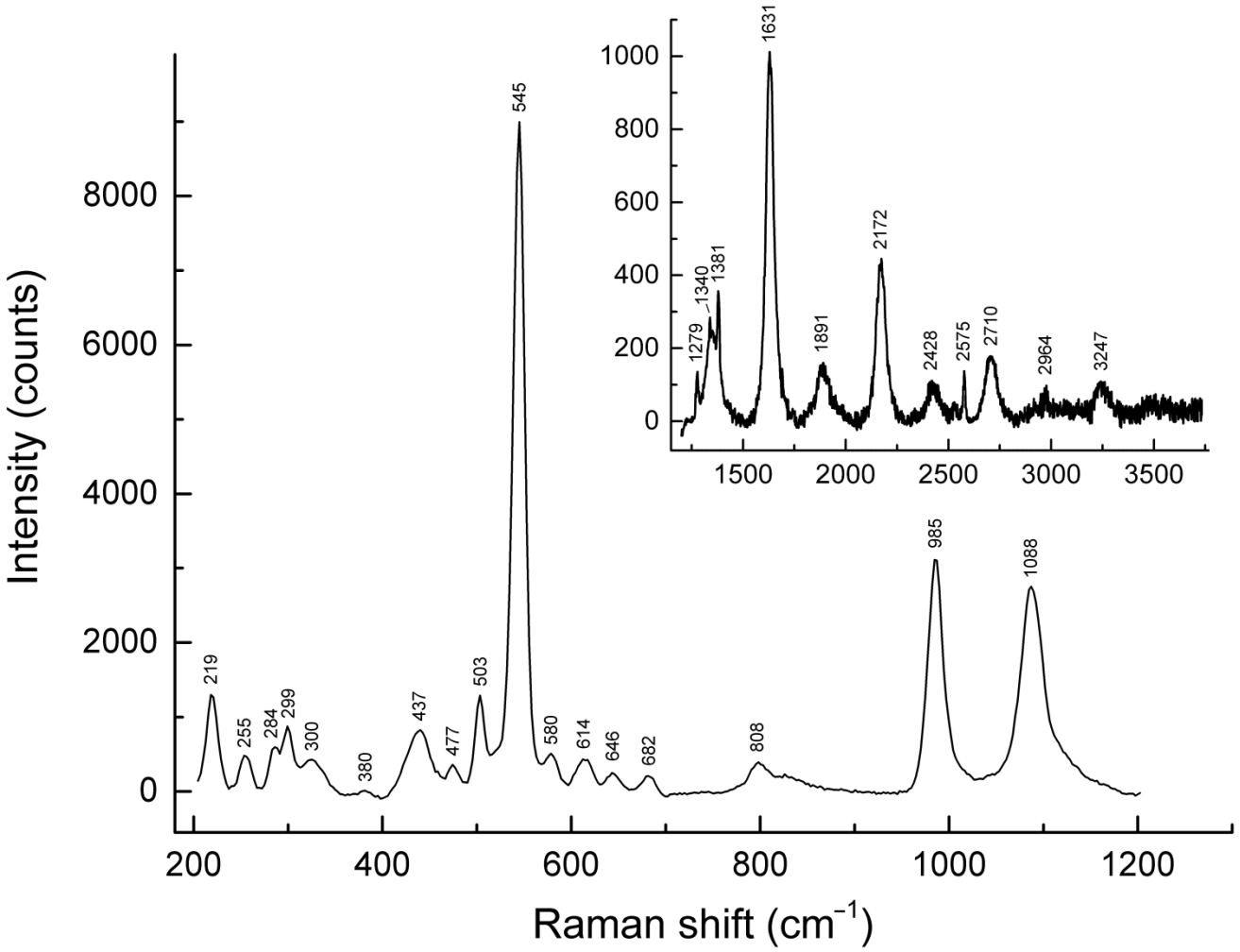

Figure 3

This is the peer-reviewed, final accepted version for American Mineralogist, published by the Mineralogical Society of America.
The published version is subject to change. Cite as Authors (Year) Title. American Mineralogist, in press.
DOI: https://doi.org/10.2138/am-2022-8598. http://www.minsocam.org/

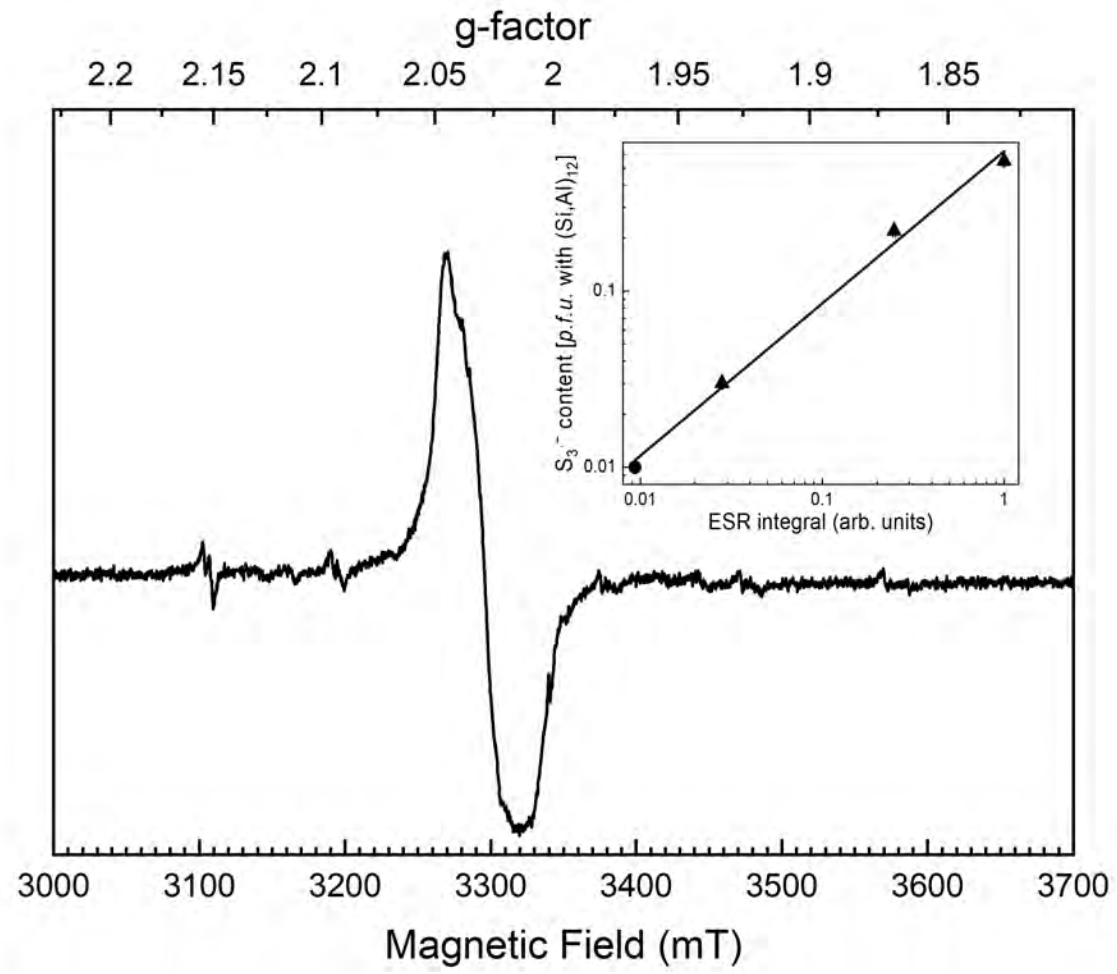

Figure 4

This is the peer-reviewed, final accepted version for American Mineralogist, published by the Mineralogical Society of America.
The published version is subject to change. Cite as Authors (Year) Title. American Mineralogist, in press.
DOI: https://doi.org/10.2138/am-2022-8598. http://www.minsocam.org/

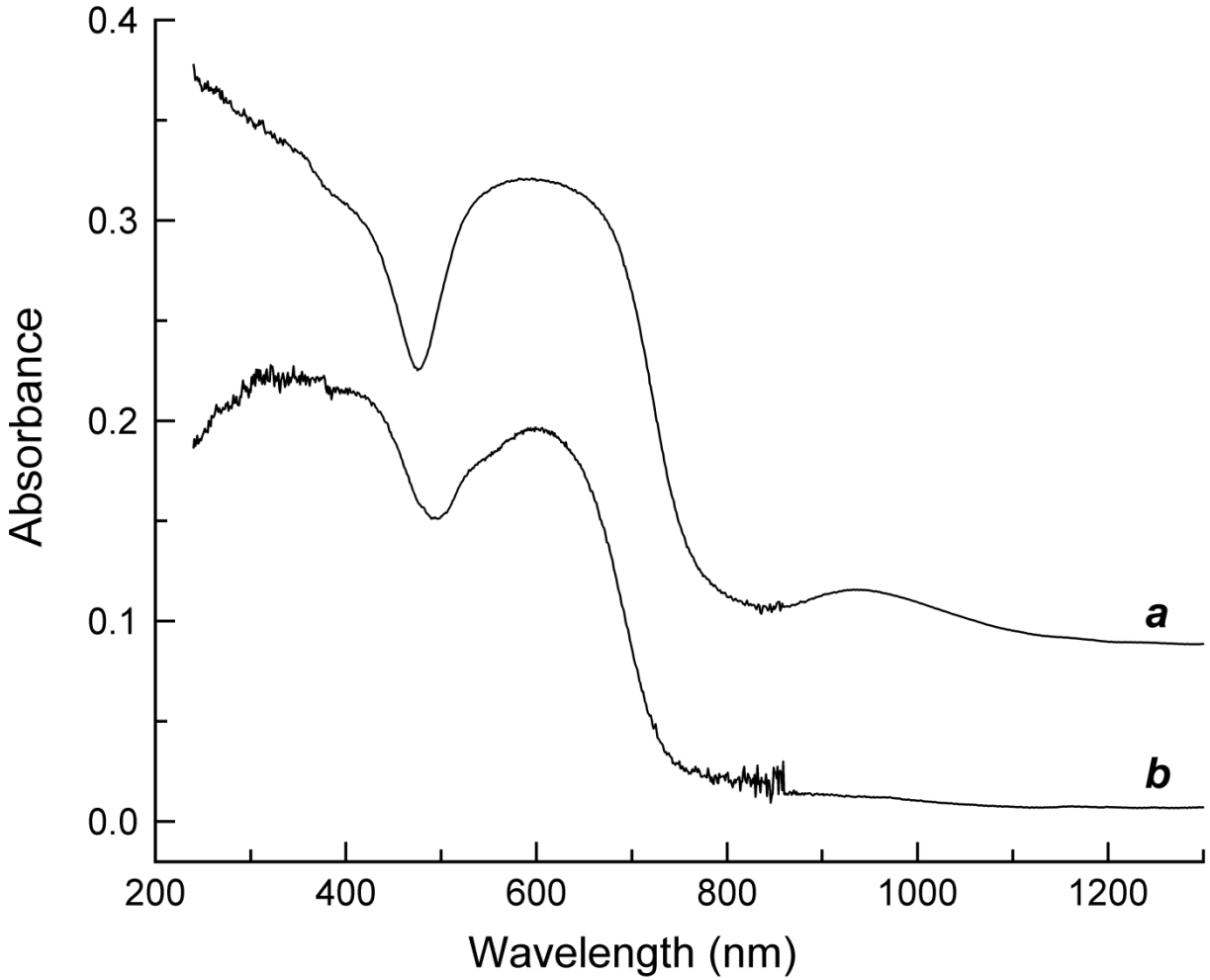

Figure 5

This is the peer-reviewed, final accepted version for American Mineralogist, published by the Mineralogical Society of America.
The published version is subject to change. Cite as Authors (Year) Title. American Mineralogist, in press.
DOI: https://doi.org/10.2138/am-2022-8598. http://www.minsocam.org/

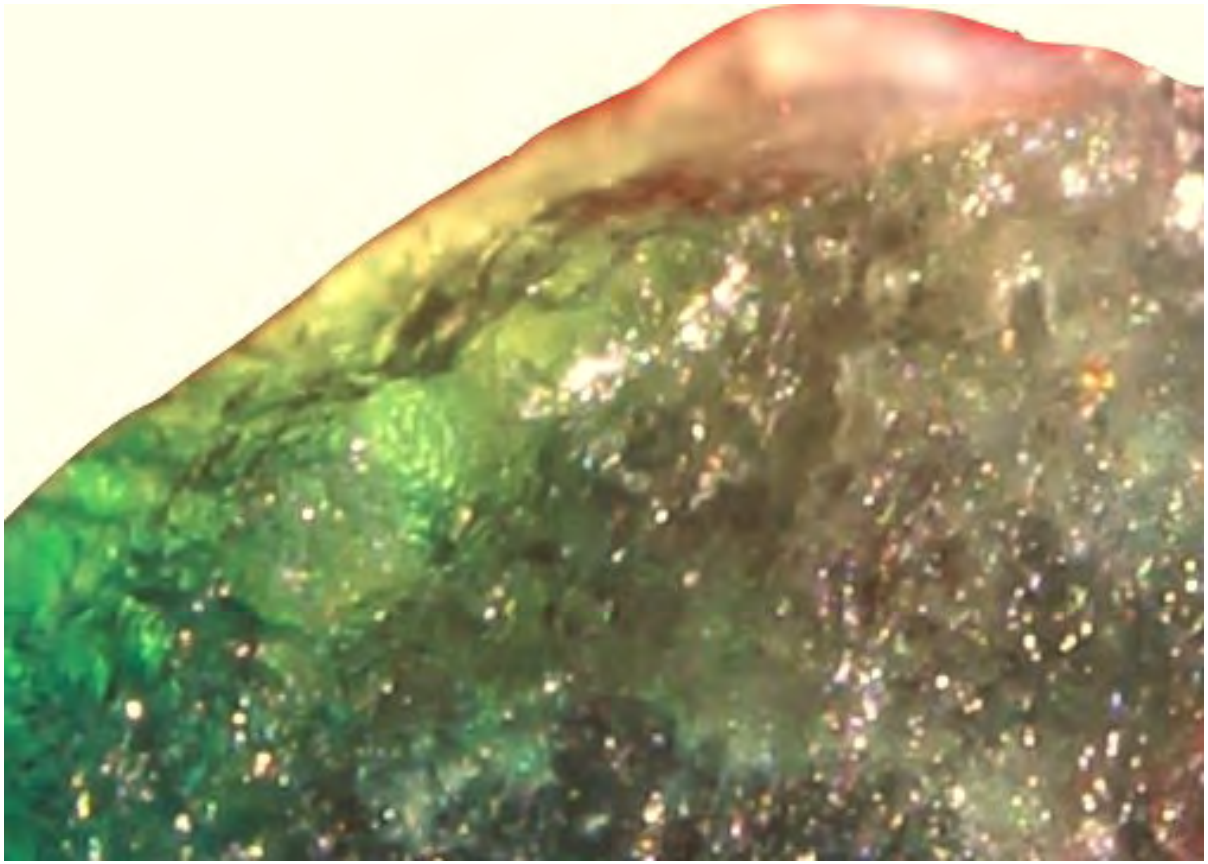

Figure 6

This is the peer-reviewed, final accepted version for American Mineralogist, published by the Mineralogical Society of America.
The published version is subject to change. Cite as Authors (Year) Title. American Mineralogist, in press.
DOI: https://doi.org/10.2138/am-2022-8598. http://www.minsocam.org/

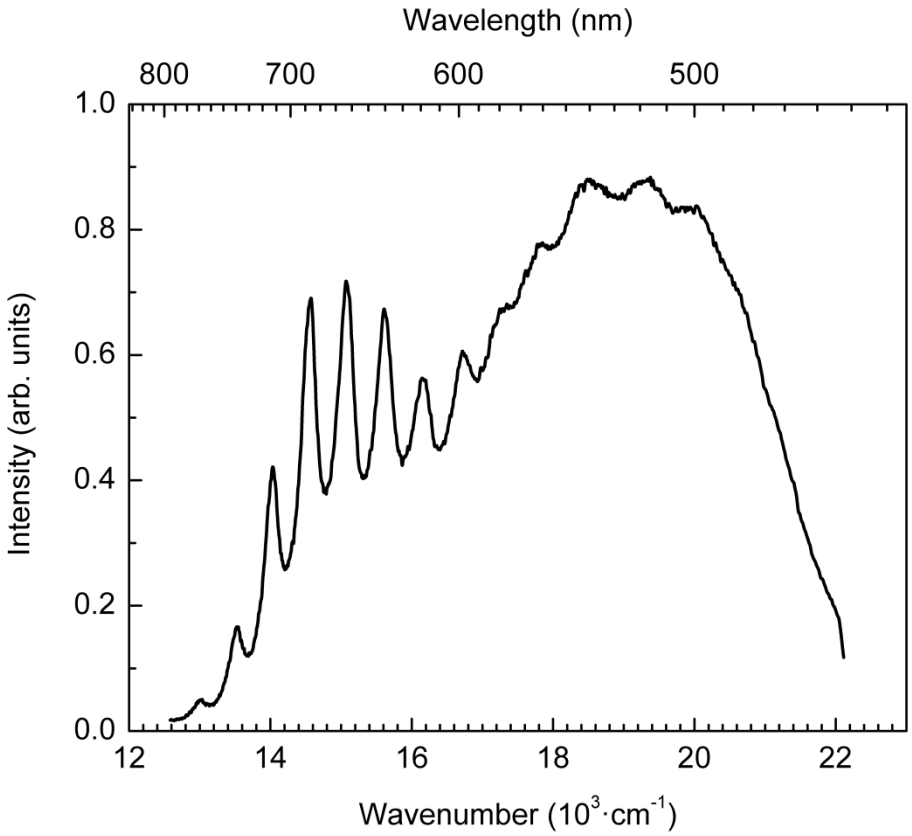

Figure 7

This is the peer-reviewed, final accepted version for American Mineralogist, published by the Mineralogical Society of America.
The published version is subject to change. Cite as Authors (Year) Title. American Mineralogist, in press.
DOI: https://doi.org/10.2138/am-2022-8598. http://www.minsocam.org/

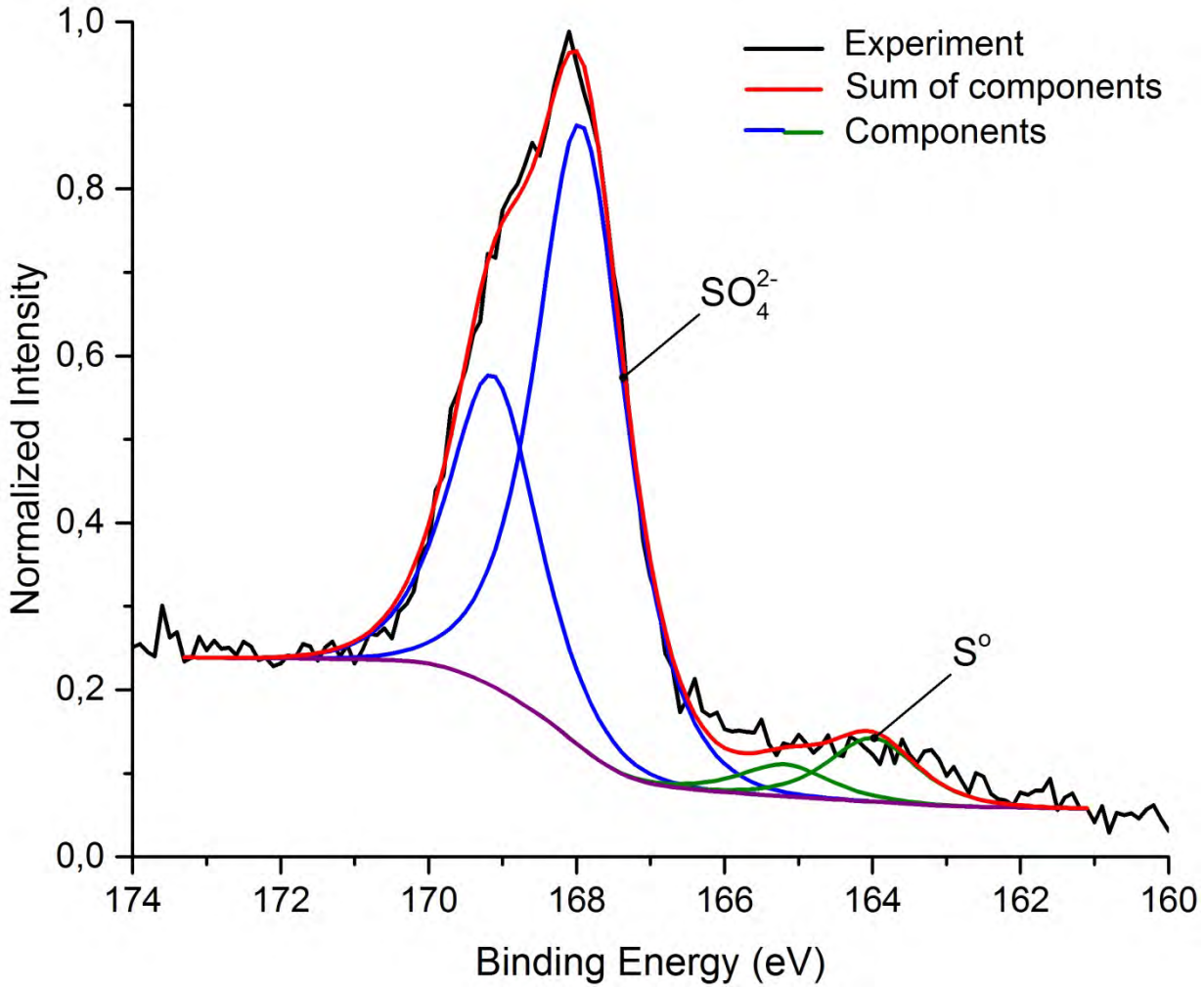

Figure 8

This is the peer-reviewed, final accepted version for American Mineralogist, published by the Mineralogical Society of America.
The published version is subject to change. Cite as Authors (Year) Title. American Mineralogist, in press.
DOI: https://doi.org/10.2138/am-2022-8598. http://www.minsocam.org/

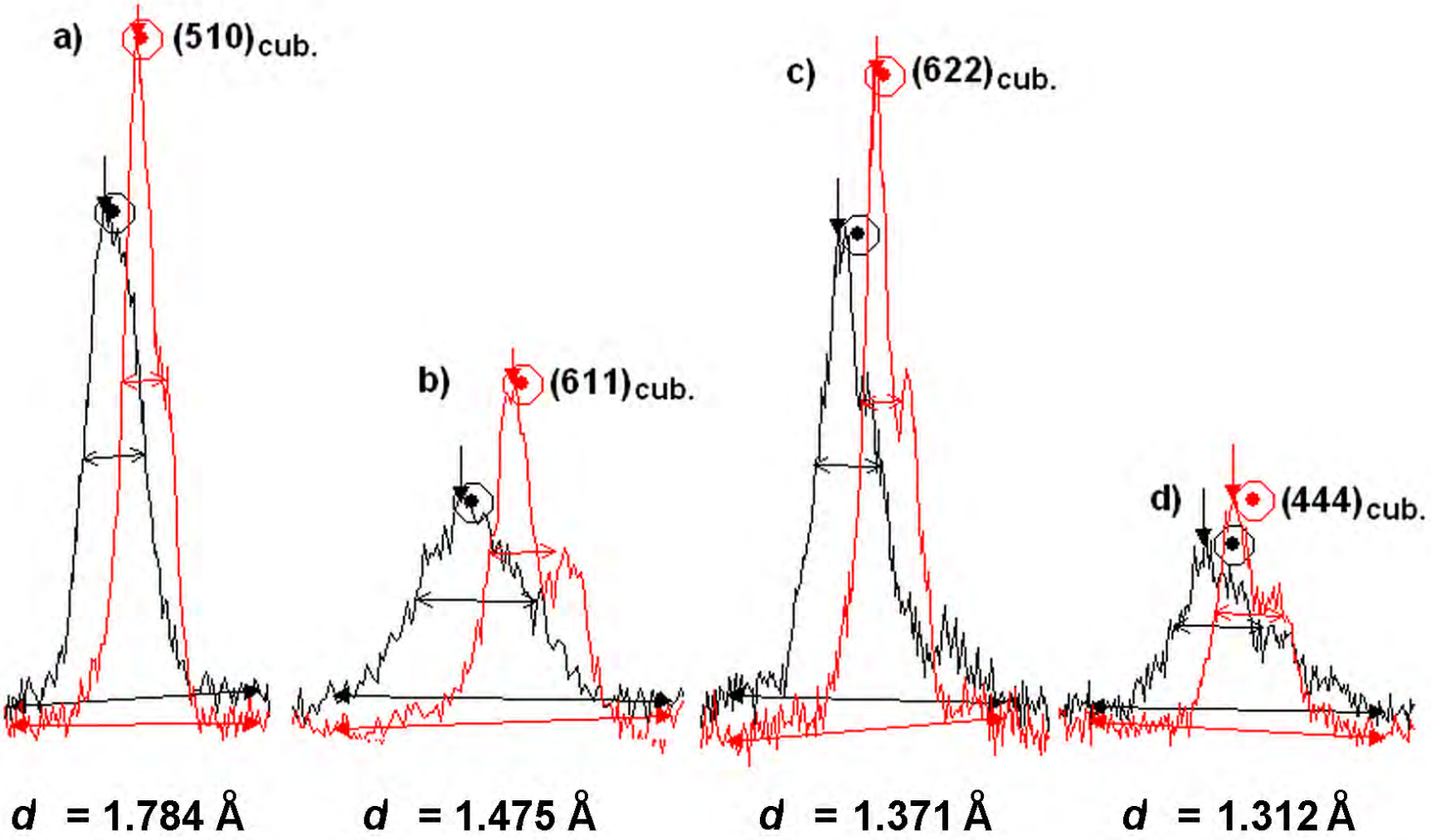

Figure 9

This is the peer-reviewed, final accepted version for American Mineralogist, published by the Mineralogical Society of America.
The published version is subject to change. Cite as Authors (Year) Title. American Mineralogist, in press.
DOI: https://doi.org/10.2138/am-2022-8598. http://www.minsocam.org/

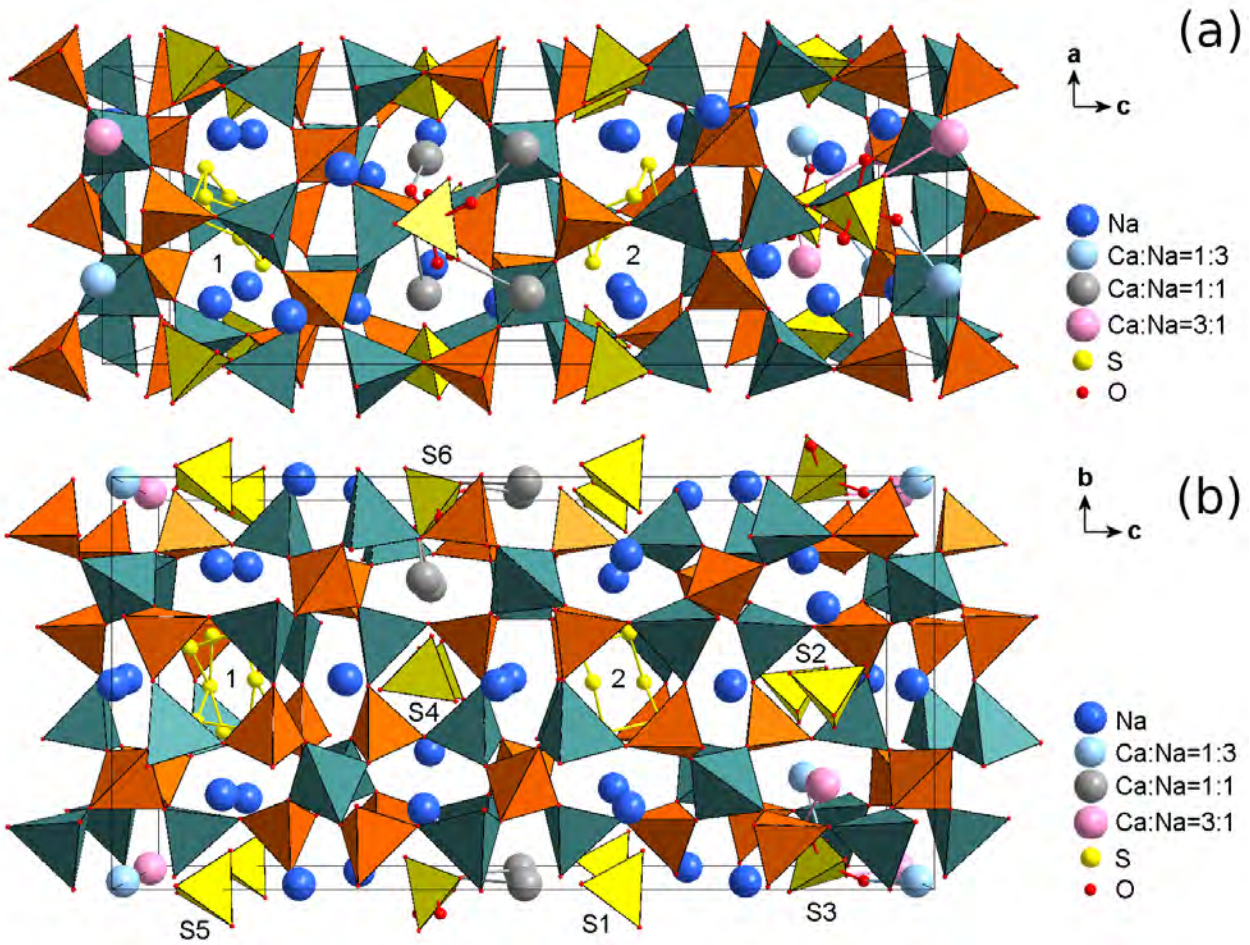

Figure 10

This is the peer-reviewed, final accepted version for American Mineralogist, published by the Mineralogical Society of America.
The published version is subject to change. Cite as Authors (Year) Title. American Mineralogist, in press.
DOI: https://doi.org/10.2138/am-2022-8598. http://www.minsocam.org/

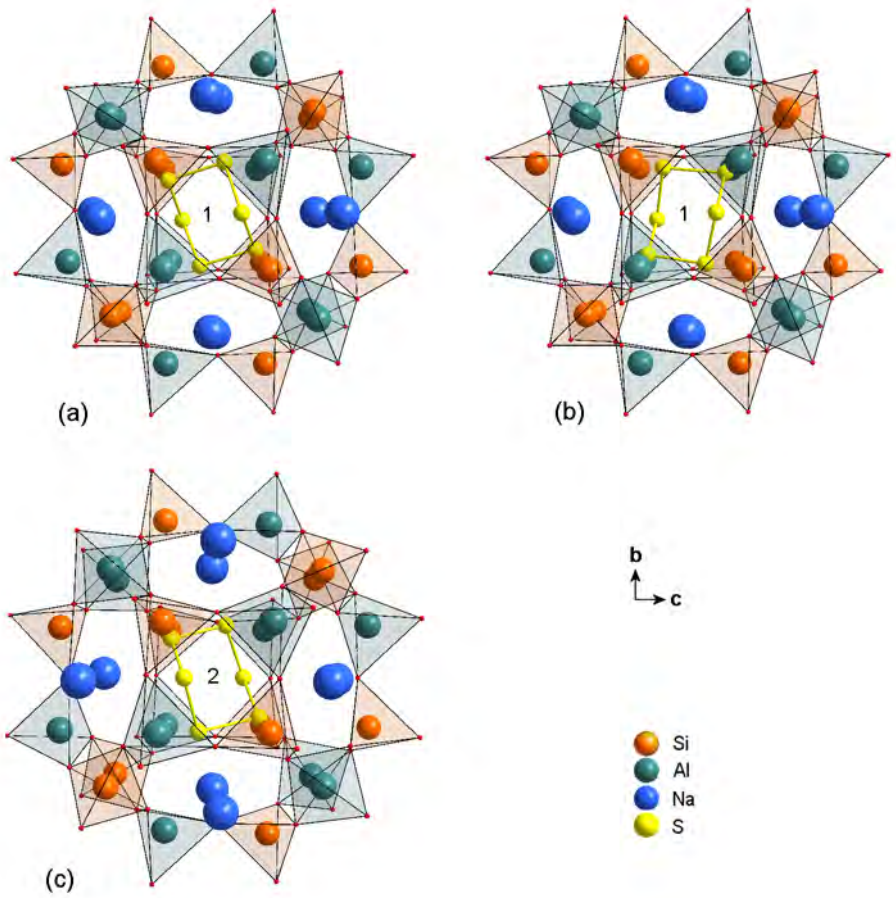

Figure 11

This is the peer-reviewed, final accepted version for American Mineralogist, published by the Mineralogical Society of America.
The published version is subject to change. Cite as Authors (Year) Title. American Mineralogist, in press.
DOI: https://doi.org/10.2138/am-2022-8598. http://www.minsocam.org/

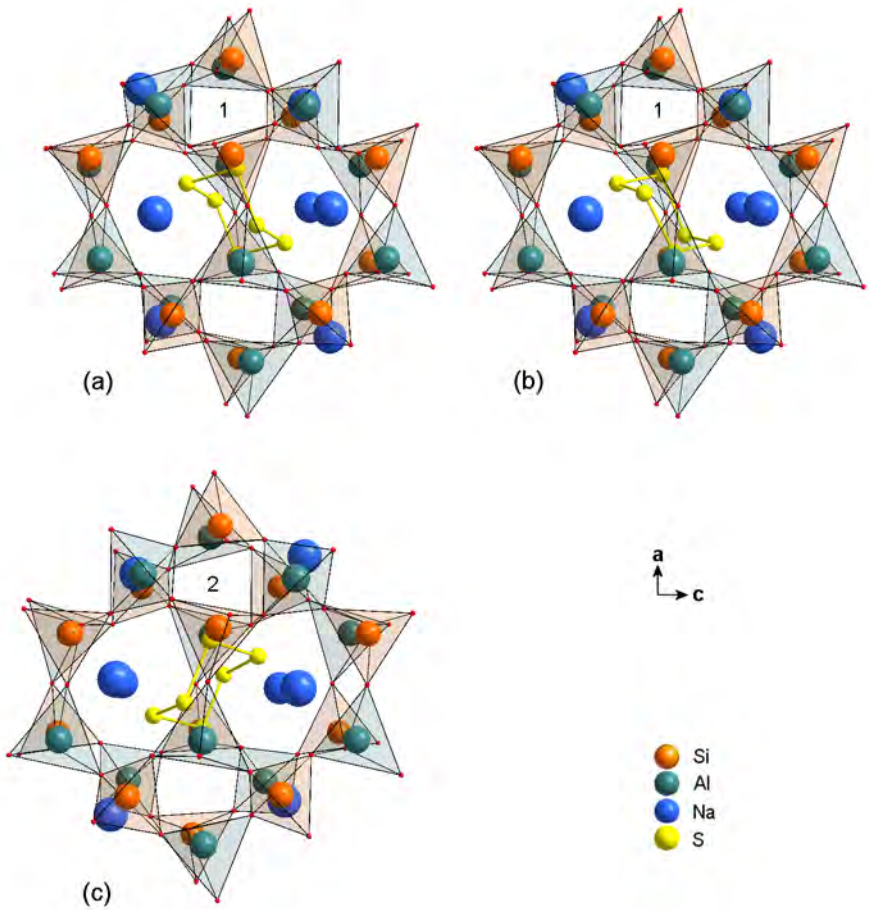

Figure 12

This is the peer-reviewed, final accepted version for American Mineralogist, published by the Mineralogical Society of America.
The published version is subject to change. Cite as Authors (Year) Title. American Mineralogist, in press.
DOI: https://doi.org/10.2138/am-2022-8598. http://www.minsocam.org/

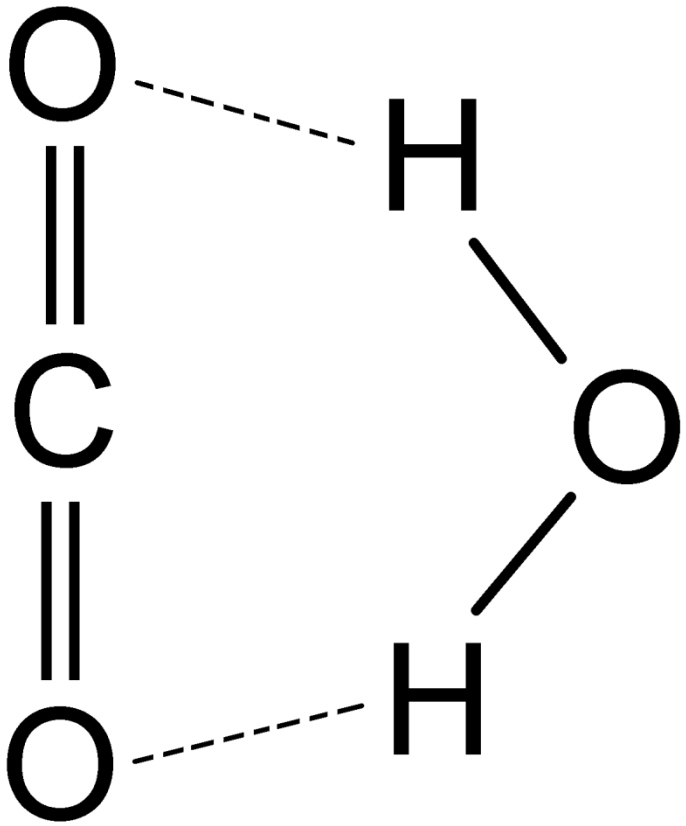

Figure 13.